Published in final edited form as:
Nature. 2016 October 27; 538(7626): 518–522. doi:10.1038/nature19801.

T cell acute leukaemia exhibits dynamic interactions with bone marrow microenvironments

Edwin D Hawkins[1,2,13,*], **Delfim Duarte**[1,*], **Olufolake Akinduro**[1,¶], **Reema A Khorshed**[1,¶], **Diana Passaro**[3,¶], **Malgorzata Nowicka**[4,5], **Lenny Straszkowski**[6], **Mark K Scott**[1,2], **Steve Rothery**[7], **Nicola Ruivo**[1], **Katie Foster**[3], **Michaela Waibel**[8,9], **Ricky W Johnstone**[8,9], **Simon J Harrison**[8,9], **David A Westerman**[8,9], **Hang Quach**[10,11], **John Gribben**[12], **Mark D Robinson**[4,5,§], **Louise E Purton**[6,11,§], **Dominique Bonnet**[3,§], and **Cristina Lo Celso**[1,13]

[1]Department of Life Sciences, Sir Alexander Fleming Building, Imperial College London, SW7 2AZ, London, United Kingdom [2]The Walter and Eliza Hall Institute of Medical Research, Melbourne, Victoria 3052, Australia [3]The Francis Crick Institute, Haematopoietic Stem Cell Laboratory, WC2A 3LY, London, UK [4]SIB Swiss Institute of Bioinformatics and Institute of Molecular Life Sciences [5]University of Zurich, 8057 Zurich, Switzerland [6]Stem Cell Regulation Unit, St Vincent's Institute of Medical Research, Fitzroy, Australia [7]Imperial College Facility for Imaging by Light Microscopy, Sir Alexander Fleming Building, Imperial College London, SW7 2AZ, London, United Kingdom [8]Sir Peter MacCallum Department of Oncology, University of Melbourne, Parkville, Victoria, Australia 3052 [9]Peter MacCallum Cancer Centre, East Melbourne Victoria, Australia 3002 [10]Department of Haematology, St. Vincent's Hospital, Fitzroy, Vic., 3065, Australia [11]Department of Medicine, The University of Melbourne, Fitzroy, Vic., 3065, Australia [12]Centre of Haemato-Oncology, Cancer Research UK Clinical Centre, Barts Cancer Institute, St Bartholomew's Hospital, Queen Mary University of London, London, UK

Abstract

It is widely accepted that complex interactions between cancer cells and their surrounding microenvironment contribute to disease development, chemo-resistance and disease relapse. In light of this observed interdependency, novel therapeutic interventions that target specific cancer stroma cell lineages and their interactions are being sought. To this end, we studied a mouse model

[13]Correspondence to Hawkins.e@wehi.edu.au, c.lo-celso@imperial.ac.uk.
*Equal contribution
¶Equal contribution
§Equal contribution

Author contributions

EH and CLC conceived the project. EH, CLC, OA, MS designed and refined the intravital imaging systems. RK designed the image analysis platform; RK, EH and DD performed all image analysis. SR designed the random data simulator. EH, DD and NR performed imaging experiments. NR maintained all animal lines. MN and MR designed and analysed microarray data. EH, MW and RJ performed experiments in Extended Data Fig. 1. DP, KF and DB designed, performed and analysed Osterix/GFP experiments. SH, DW and JG provided human T-ALL samples. LS and LP performed histological analysis of human BM trephines. HQ funded human biopsy studies. DP and DB designed and DP performed the human T-ALL xenograft experiments and analysed data. EH, DD and CLC analysed data and wrote the manuscript. Every author contributed revisions to the manuscript.

Competing financial interests

The authors have no competing financial interests regarding to the work in this manuscript.

Europe PMC Funders Author Manuscripts

of human T cell acute lymphoblastic leukaemia (T-ALL) and used intravital microscopy to monitor the progression of disease within the bone marrow at both the tissue-wide and single cell level over time, from bone marrow seeding to development/selection of chemo-resistance. We observed highly dynamic cellular interactions and promiscuous distribution of leukaemia cells that migrated across the bone marrow, without showing any preferential association with bone marrow sub-compartments. Unexpectedly, this behaviour was maintained throughout disease development, from the earliest bone marrow seeding to response and resistance to chemotherapy. Our results reveal that T-ALL cells do not depend on specific bone marrow microenvironments for propagation of disease, nor for the selection of chemo-resistant clones, suggesting a stochastic mechanism underlies these processes. Yet, while T-ALL infiltration and progression are independent of the stroma, accumulated disease burden leads to rapid, selective remodelling of the endosteal space, resulting in a complete loss of mature osteoblastic cells whilst perivascular cells are maintained. This outcome leads to a shift in the balance of endogenous bone marrow stroma, towards a composition associated with less efficient haematopoietic stem cell function1. This novel, dynamic analysis of T-ALL interactions with the bone marrow microenvironment *in vivo*, supported by evidence from human T-ALL samples, highlights that future therapeutic interventions should target the migration and promiscuous interactions of cancer cells with the surrounding microenvironment, rather than specific bone marrow stroma, in order to combat the invasion by and survival of chemo-resistant T-ALL cells.

The importance of cancer cell interactions with their surrounding microenvironment has gained increased attention due to the hypothesis that specific supportive cells may regulate quiescence, survival and self-renewal of cancer cells themselves. This relationship may underlie a critical mechanism that facilitates both the initiation of disease and chemo-resistance. Leukaemia develops within the bone marrow (BM), where it has been suggested to take part in complex crosstalk that in some cases results in microenvironment remodelling2–8. Therapeutic targeting of leukaemia-supportive niches has been proposed9,10, therefore it is critical that we understand both the spatial and kinetic nature of leukaemia-BM interactions. However, our current knowledge of leukaemia biology is predominantly derived from *ex vivo* flow cytometric analysis, and static images that cannot capture information on the location and dynamics of leukaemia interactions with BM structures and cells over time.

We studied a Notch-driven mouse model of T cell acute lymphoblastic leukaemia (T-ALL), which recapitulates human disease both phenotypically (Extended Data Fig. 1) and genetically11,12. 25% paediatric and 40% adult T-ALL patients develop aggressive relapsed disease originating from chemo-resistant clones13. Thus, there is a pressing need to understand if T-ALL cells migrate to, and interact with particular BM stroma during the propagation of disease and/or selection of chemo-resistance, or if T-ALL can remodel the BM microenvironment in its favour.

To address these questions, we monitored leukaemia growth in mouse calvarium bone marrow by intravital microscopy14–16. We used a tile-based imaging approach akin to Google Earth that allows tissue-wide visualisation of heterogeneous BM microenvironments (Fig. 1a, b) whilst maintaining resolution that permits measurement of single leukaemia cell

interactions with BM cells and structures by time-lapse microscopy15 (Fig. 1c and Supplementary Video 1). To systematically characterise T-ALL interactions *in vivo*, we injected transformed leukaemic cells isolated from primary hosts into secondary recipients, and observed highly synchronous disease progression (Fig. 1d and Extended Data Fig. 1). In secondary recipients, T-ALL preferentially infiltrated the BM before expansion to peripheral lymphoid organs (Extended Data Fig. 1). This is consistent with expression of CXCR4, albeit at variable levels, on leukaemic cells (Extended Data Fig. 1). We visualised T-ALL cells relative to osteoblasts (GFP or CFP positive in Col2.3-GFP/CFP reporter mice17,18), perivascular mesenchymal stem/progenitor cells (GFP positive in nestin-GFP reporter mice19) and vasculature (by injecting Cy5 dextran) in cohorts of recipient mice during disease progression and treatment (Fig. 1d).

By day 10 post-transplantation we could reproducibly observe single, sparse T-ALL cells in the BM at a frequency of 1-30 cells per calvarium (Fig. 1e, f). We measured the proximity of leukaemia cells to osteoblastic and nestin-GFP$^+$ cells and vasculature. We used randomly positioned dots as a control for the specificity of observed associations, as these do not possess any inherent ability to localise to a particular BM stroma component (Fig. 1g). The distribution of T-ALL cells was equivalent to that of the random dots and the actual distances recorded inversely correlated with the abundance of each component (Fig. 1g-j). These results demonstrate that seeding T-ALL in the BM is stochastically distributed relative to osteoblasts, nestin-GFP$^+$ cells and vasculature.

To determine whether T-ALL expansion was supported by specific constituents of the BM, we monitored the dynamics of single T-ALL cells (Fig. 2a) for 3 hours (Fig. 2b, c, Extended Data Fig. 2 and Supplementary Videos 2 and 3). This revealed that the vast majority of T-ALL cells were motile, in stark contrast with previous observations of transplanted haematopoietic stem cells in BM15, and that movement was rarely restricted to the proximity of any specific cell types or structures (Position 2 and 3 in Fig. 2b, c, and Supplementary Videos 2 and 3). Notably, the speed of any given cell over time was also heterogeneous, and thus no single migratory behaviour was associated with osteoblastic, nestin-GFP$^+$ cells or vasculature (Fig. 2c, Extended Data Fig. 2 and Supplementary Videos 2 and 3). Tracking single T-ALL cells enabled us to measure the location of mitotic events, revealing the same stochastic distribution of dividing cells and suggesting that proximity to these stroma components is not key for T-ALL expansion (Fig. 2d, e, Extended Data Fig. 2, Supplementary Videos 2 and 3). Additionally, daughter cells migrated large distances following division, illustrating that clones and their progeny are not restricted to foci within the local microenvironment (Fig. 2c and Supplementary Video 2, position 3). These observations were consistent with tilescans performed at later stages of BM colonisation (day 12-18 post transplantation), where we detected pockets of high and low infiltration juxtaposed in all types of microenvironments (Extended Data Fig. 3 and 4). Interestingly, the motility patterns displayed by single, isolated cells were also consistently observed when tracking individual cells located in densely infiltrated areas (Supplementary Video 4). Combined, these analyses demonstrate that T-ALL seeding and colonisation of BM do not select for, or depend on specific BM stroma.

The question remained whether certain BM regions could create “hotspots” for chemo-resistance through provision of a protective environment. To address this issue, we adapted our imaging protocol to follow the same BM areas over multiple days to track leukaemia dynamics from complete BM infiltration and throughout therapy. We used the lock-and-key mechanism of the imaging window to precisely re-position mice on the microscope stage over multiple imaging sessions. Mice were tilescanned 18 days post T-ALL transplantation to confirm full BM infiltration. Dexamethasone was then administered daily (Fig. 3a), and immediately after the third therapy dose we observed a staggering reduction in disease burden20 (Fig. 3b-d and Extended Data Fig. 5a-b), while non-leukaemic, dexamethasone-treated control mice maintained robust BM and stroma cellularity (Extended Data Fig. 5d-e). Strikingly, surviving cells were scattered throughout the BM space and not preferentially associated with osteoblastic, nestin-GFP$^+$ cells or vasculature compared to simulated data (Fig. 3b-f, Extended Data Fig 5a-c).

To test whether initial T-ALL loss was independent from specific stroma components, we increased the imaging temporal resolution to include the first day of treatment. The distribution of T-ALL cells was maintained as disease gradually succumbed to therapy (Extended Data Fig. 6). In contrast to predictions based on previous publications3,9,10, time-lapse imaging immediately after administration of the third dose of dexamethasone demonstrated that single surviving cells were highly migratory and did not maintain long-lasting associations with osteoblastic (Fig 3g, h and Supplementary Video 5) or nestin-GFP$^+$ cells (Supplementary Video 6). Furthermore, surviving cells travelled at significantly faster speeds than early infiltrating cells (days 10-15) (Fig. 3m). Finally, residual T-ALL cells were still capable of undergoing division (Fig. 3g, Supplementary Videos 5 and 6) at times when other cells within the same mouse were still undergoing death (Supplementary Video 6). This behaviour, coupled with the observation that mice maintained on dexamethasone for a 7-day period harbored an almost completely repopulated BM space (Extended Data Fig. 7a), suggests these cells were genuinely resistant to dexamethasone.

Collectively, these data oppose the prevailing hypothesis that therapy-resistant leukaemic cells depend on a particular microenvironment for survival. To investigate this proposed paradigm, we compared the gene expression profile of T-ALL cells purified at full infiltration to those isolated from mice 7-10 days after initiation of dexamethasone treatment, when surviving cells have re-colonised the BM (Extended Data Fig. 7a). Gene expression profiles of all T-ALL samples were more heterogeneous compared to control T cells (CD4$^+$ and CD8$^+$), T cell progenitor (CD4$^+$CD8$^+$ thymocytes) and whole BM populations as expected based on inter-clone variation in leukaemia cells21. The transcriptome of resistant cells overlapped with that of T-ALL cells pre-treatment (Extended Data Fig. 7c). Indeed, only 79 genes were differentially expressed in the post-treatment group and, consistent with our intravital imaging data, none of the differentially expressed genes were related to known cell-niche interaction candidates (Supplementary Table 1 and Extended Data Fig. 7b). Together, our imaging and gene expression data suggest that dexamethasone treatment does not select for a subpopulation of T-ALL cells that have been directed to a specific niche.

To investigate the significance of these data in a human context, we assessed the migratory behaviour of xenotransplanted primary human T-ALL (Supplementary Table 2) in NOD/SCID/γ mice. Following dexamethasone treatment, even human wild-type Notch receptor T-ALL cells exhibited migratory behaviour equivalent to murine cells (Extended Data Fig. 8a-d and Supplementary Video 7). We noted an even distribution of quiescent cells throughout the BM as measured by Ki-67 staining (Extended Data Fig. 8e-f). To test whether the migratory behaviour was a specific trait induced by dexamethasone, we treated murine T-ALL burdened animals with vincristine. The T-ALL response followed similar kinetics to that of dexamethasone-treated animals. Enhanced migration of resistant cells and cell division events were evident immediately after the third dose of vincristine (Figure 3i, j, m and Supplementary Video 8). This behaviour was even more pronounced when we combined dexamethasone, vincristine and L-asparaginase (Fig. 3k-m, Extended Data Fig. 9 and Supplementary video 9). In this context, we observed the highest migration speed of all therapies tested, despite over 50% of surviving cells being in G0 (Figure 3n, o), demonstrating quiescence is not a feature of niche-restricted immotile cells following chemotherapy. These findings were universal in all therapies tested in our studies, suggesting migration and lack of long-lasting interactions with the surrounding microenvironment are conserved features of chemo-resistance in T-ALL.

To assay whether T-ALL may affect BM structures, we performed time-lapse imaging in heavily disease-burdened, untreated mice. After day 18 we observed striking remodelling of osteoblasts (Fig. 4a, b). A 9-hour period of time-lapse imaging after full infiltration (day 19 onwards) revealed that osteoblastic cells underwent dramatic shrinking and blebbing (Fig. 4a and Supplementary Video 10), in stark contrast to early stages of disease (Supplementary Video 1) and to control Col2.3-GFP mice reconstituted with red fluorescent healthy BM (Fig. 4a, b, Extended Data Fig. 10a, b and Supplementary Video 10). TUNEL and cleaved caspase-3 histological stainings indicated osteoblasts were undergoing apoptosis (Fig. 4c). The loss of osteoblasts was so dramatic that virtually no GFP^+ osteoblasts remained apparent by days 22-25 post transplantation (Fig. 4b, d). Similar results were also found for $osterix^+$ osteo-progenitors (Fig. 4f), however, nestin-GFP^+ cells were maintained (Fig. 4e and Extended Data Fig. 10c, d), and blood vessels could still be visualised (Extended Data Fig. 10e). Importantly, these findings were consistent in analyses performed using human T-ALL samples (Supplementary Table 2). We observed a significant reduction in $osterix^+$ osteo-progenitors in NOD/SCID/γ recipient mice xenotransplanted with human T-ALL samples (Fig. 4f). Additionally, histological analysis of BM trephine biopsies from T-ALL patients with greater than 75% infiltration demonstrated an almost complete loss of osteoblasts (Fig. 4g).

In summary, we demonstrate T-ALL infiltrates the BM and survives chemotherapy independently of stable interactions with specific microenvironments. However, T-ALL has a profound effect on osteoblastic cells. Our results suggest that to avoid the development of chemo-resistance, novel therapeutic interventions may not need to target specific BM stroma components, but rather the ability of T-ALL cells to interact with and migrate through the BM. Our studies also reveal that T-ALL has the intrinsic potential to remodel the BM microenvironment via apoptosis throughout the osteolineage. As these cells are associated with haematopoietic fitness14,22,23, including in the context of leukaemia1,2,24, the

remodelling we uncovered may contribute to the loss of healthy haematopoiesis observed in leukaemia patients1,2. Collectively, our observations suggest that a shift in therapeutic design may be advisable, such that any intervention targeting osteoblastic cells should focus on promoting survival of this lineage, rather than seeking to modulate a direct influence of the BM on the cancer itself. Therefore, a better focus for novel anti-cancer therapeutics may be on disrupting the ability of T-ALL cells to interact transiently with multiple components of the BM microenvironment.

Online Materials and Methods

Mice

All animal experimentation in this study was approved and performed according to the standards of the animal ethics committee at Imperial College London, UK and to UK home office regulations (ASPA 1986). C57Bl/6 mice were purchased from Harlan UK Ltd; Col2.3-GFP, Col2.3-CFP18, Nestin-GFP and mTmG26 mice were bred and housed at Imperial College London, UK. For imaging experiments, female Col2.3-GFP and Nestin-GFP mice >8 weeks old were used. Osterix-CreGFP mice were provided by A. McMahon and backcrossed over 8 generations into NSG mice and maintained at the Francis Crick Institute, Cancer Research UK27. Equal proportions of male and female Osterix-CreGFP mice aged 11-14 weeks were used.

Generation of murine T-ALL disease

T-ALL was generated as previously described in28. Briefly, timed matings were established between C57/Bl6 mice and embryos harvested at day E14.5. Single cell suspensions were prepared from whole foetal livers isolated from the embryos. Suspensions were cultured in IL-3, IL-6, and stem cell factor conditioned media with 20% FCS for 3 days. Lin-xE cells were transfected by calcium phosphate with MigR1 plasmids containing either DsRed only or DsRed with NotchICNΔRamΔP as originally described in29. We also used GFP tagged plasmids when required. Supernatants containing recombinant retrovirus were removed and spun by centrifugation onto non-tissue culture treated plates coated with 15ug/ml retronectin (Takara Clontech, CA). Foetal liver cells were cultured in the presence of virus for 3 days and transduction assessed by flow cytometry. Primary lethally irradiated recipient mice (two doses of 5.5Gy administered greater than three hours apart) were transplanted with $1x10^6$ $DsRed^{+ve}$ foetal liver cells by intravenous injection into the tail vein. Recipient mice were maintained on baytril treated water to prevent infection for >6 weeks post transplantation. Cohorts of reconstituted mice were the result of 3 independent foetal liver isolations and 3 independent transfections. Transformation of Notch-transduced non-malignant cells is highly heterogeneous *in vivo*, with onset of primary disease ranging from 6-25 weeks29 (Extended Data Fig. 1). >4 weeks post reconstitution, peripheral blood was isolated from mice, red blood cells were lysed, and successful reconstitution determined by presence of $DsRed^+$ cells. Mice reconstituted with NotchICNΔRamΔP transduced foetal livers were monitored daily for signs of leukaemia onset or other signs of ill health. Mice were euthanized when any one, or combination of the following signs were observed: hunched posture, laboured breathing, weight loss, enlarged lymph nodes and/or spleen, peripheral white blood cell cellularity of 13 $x10^9$/L or greater. No experiment exceeded the tumour

burden approved by the Home Office and Imperial College ethics committee. Peripheral lymphoid organs were analysed by flow cytometry for DsRed or GFP, CXCR4, CD3, CD4 and CD8 expression. All FACS data was collected on a Fortessa flow cytometer (BD Biosciences, CA). Secondary recipients were sub-lethally irradiated (two doses of 3Gy administered greater than three hours apart) and injected with 10,000 thawed, Ficoll purified T-ALL blasts and monitored as described above. In selected cases 10,000 secondary T-ALL cells were transplanted into tertiary recipients. For therapy experiments, mice were injected I.V daily with 15mg/kg dexamethasone sodium phosphate30,31 (Sellekchem, MA) alone, 0.15mg/kg vincristine sulfate salt (Sigma) alone or with a combination of 15mg/kg dexamethasone, 0.15mg/kg vincristine and 1,000 IU/kg L-asparaginase (medac; obtained from the Imperial College Healthcare NHS Trust Pharmacy).

Bone marrow chimaeras

Reconstitution with MigR1 DsRed transduced cells yields <50% chimerism. For this reason, analysis of healthy BM cells by microscopy is inaccurate. Therefore, to obtain >95% chimerism of healthy, red fluorescent BM to be used for imaging control experiments, whole BM mononuclear cells were isolated from femurs, hips and tibia of mTmG donor mice, suspended in phosphate balanced salt solution and administered intravenously to recipient mice at a dose of $2x10^6$ cells/mouse. Recipient Col2.3-GFP or C57Bl/6 mice had been lethally irradiated (two doses of 5.5Gy irradiation greater than 3 hours apart) immediately prior to the transplant, and were maintained on baytril treated water to prevent infection >6 weeks post transplantation.

Intravital microscopy

Intravital microscopy was performed using a Leica SP5 and a Zeiss LSM 780 upright confocal microscope with a motorised stage. The SP5 was fitted with the following lasers: Argon, 546, 633 and a tunable infrared multiphoton laser (Spectraphysics Mai Tai 690-1020). The Zeiss LSM 780 was fitted with the following lasers: Argon, 561, 633 and a tunable infrared multiphoton laser (Spectraphysics Mai Tai DeepSee 690-1040). Signal was visualised with a Leica HCX IRAPO L 25x water immersion lens (0.95 N.A) and a W Plan-Apochromat 20x DIC water immersion lens (1.0 N.A). Collagen bone second harmonic generation signal and GFP signal were generated through excitation at 840 nm and detected with external detectors. Internal detectors were used to collect DsRed and Cy5 signal (and on some occasions, GFP). Prior to surgery, mice were administered analgesia with buprenorphine (0.1mg/kg I.P). Anaesthesia was induced in mice with 4% isoflurane mixed with pure oxygen. This was gradually reduced to approximately 1% as anaesthesia stabilised. Surgery to attach the headpiece was then performed as described in16. Large 3 dimensional ‘tilescans’ of the entire BM cavity space were acquired by stitching adjacent, high-resolution Z-stack images using a surgically implanted imaging window that ensures steady positioning of mice on the microscope. The calvarium has been demonstrated to be equivalent to the long bones such as the femur with regards to haematopoietic stem cell frequency, function and localisation14,22, and is the only bone marrow compartment that allows longitudinal imaging through minimally invasive surgery16,32. Blood vessels were highlighted by I.V. injection of 50μl of 8μg/ml 500kD Cy5-Dextran (Nanocs, MA). Cy5 Dextran was re-injected every one-two hours to maintain blood vessel signal and cross

reference for registration of blood vessel data in time-lapse analysis. For repeated imaging, protective intrasite gel (Smith & Nephew, UK) was applied to the imaging window to preserve the bone integrity and prevent scar formation. The window was bandaged, and mice were allowed to recover from anaesthesia. Due to the lock-and-key mechanism of the imaging window16, mice could then be re-anaesthetised and accurately repositioned on the microscope stage and the same BM areas re-imaged. After each imaging, analgesia was administered via oral buprenorphine in raspberry jelly at a dose of approximately 0.8mg/kg.

Image quantification

Microscopy data was processed using multiple platforms. Tilescans were stitched using Leica Application Systems (LAS, Leica Microsystems, Germany) and ZEN black (Zeiss, Germany) softwares. Raw data was visualised and processed using Fiji/Image J. Simulated data was prepared using FIJI macro to create, and overlay z-stack images on original tilescan data. Using the internal random number algorithm, spheres matching the size of T-ALL cells (11-15μm) were placed at random x,y,z co-ordinates. Simulated data FIJI macro is available on request. Automated cell segmentation, distance and volume measurements were performed in Definiens (Definiens Developer 64, Germany) using local heterogeneity segmentation25 to isolate osteoblast and Nestin cells as well as vasculature, and a combination of seed detection algorithm and morphological growing and shrinking operations to detect leukaemia cells. Definiens rulesets for these functions are available upon request. Distance measurements from this segmentation were performed as described in25. Cell tracking was performed using Imaris (Bitplane, Switzerland) and the FIJI plugin MTrackJ. For accuracy in cell tracking data, videos were registered when required before using 4D data protocols implemented in Fiji33. 3D data rendering and measurement of cell division distances were performed in Volocity (Perkin Elmer, MA) and Definiens (Definiens Developer 64, Germany).

Microarrays

T-ALL samples were harvested from bone marrow and FACS sorted based on fluorescent protein expression (DsRed or GFP) unless infiltration of bone marrow was complete. Control samples for microarray were prepared by FACS sorting for splenic $CD4^+$ T cells, $CD8^+$ T cells and $CD4^+CD8^+$ thymocytes from 8-14 week female C57Bl/6 mice. RNA was purified from samples using the Qiagen RNeasy mini kit (Netherlands) as per the manufactures instructions. Purified RNA was prepared for hybridisation using the Genechip® WT Plus reagent kit (Affymetrix, CA, USA) as per the manufactures instructions and hybridised with genechip® Mouse gene 2.0 ST array (Affymetrix, CA, USA) by the MRC Genomics facility (Imperial college London, UK). Analysis was performed using R version 3.1.1. Data was normalised and summarised to “core” level using the RMA method from the oligo package (version 1.30.0)34. Annotation was downloaded from the Affymetrix NetAffx Query website. Differential expression was determined using limma version 3.22.735. Genes with Benjamini-Hochberg-adjusted p-value < 0.05 and absolute log-fold-change > 1 were deemed significant. Heatmaps of gene expression were generated with pheatmap package version 1.0.2. Gene expression data are available on ArrayExpress (accession number E-MTAB-4889).

Human T-ALL xenografts

Primary human T-ALL samples were obtained from the Barts Hospital (London, UK) after informed consent via a protocol approved by the East London Research Ethics Committee and carried out in accordance with the principles of the Helsinki declaration (see Supplementary Table 2 for details), prior to treatment being administered to the patients. Primary cells from two distinct patients were immunophenotyped, and $CD45^{+}/CD7^{+}/CD4^{-/low}/CD8^{-/low}$ cells sorted and infused I.V. in a non-conditioned Osterix-CreGFP/NOD/SCID/γ recipient mice. Primary xenograft transplantation was assessed via peripheral blood sampling and/or bone marrow aspiration. Bone marrow and spleen-derived primary xenografts were infused I.V. in non-conditioned NOD/SCID/γ secondary recipient mice for therapy experiments. Intravital imaging was performed as described above. Human T-ALL cells were labelled by injecting 10 μg of PE-conjugated human CD45 antibody (clone HI30, Biolegend) 15-30 minutes prior to the imaging session. For dexamethasone therapy experiments, mice were treated with daily injections of 15mg/kg I.V31. Number of human T-ALL cells in therapy experiments was quantified using reference beads as described in36.

Immunofluorescence

Hips and tibias were harvested and post-fixed overnight in periodate-lysine-paraformaldehyde fixative, at 4ºC. Bones were then washed with 0.1M phosphate buffer, cryoprotected in sucrose (10-30% gradient), for 48h, frozen in optimal cutting temperature compound (TissueTek) and stored at -80ºC. Sections were cut in a Leica Cryostat, using the Cryojane tape transfer system (Leica microsystems) and stored at -80ºC. For staining, slides were re-hydrated in PBS, permeabilised in 0.1% Triton X-100, blocked in 5% goat serum and incubated with primary antibodies overnight, at 4 °C. After washing in PBS, slides were incubated with secondary antibodies, counter-stained with 4,6-diamidino-2-phenylindole (DAPI, Invitrogen), washed in 0.1% Triton X-100 and mounted using Prolong Diamond antifade (Invitrogen). The following antibodies were used: Alexa Fluor 647 mouse anti-Ki-67 (B56, BD Biosciences, 1:50), PE-conjugated human CD45 antibody (HI30, BD Biosciences, 1:100), rabbit anti-cleaved caspase-3 (Asp175, Cell Signaling, 1:100), goat anti-rabbit IgG Alexa Fluor 633 (Life Technologies, 1:400). Terminal deoxynucleotidyl transferase dUTP nick end labeling (TUNEL) labelling was performed to detect apoptotic cells, according to the manufacturer's instructions (DeadEnd Colorimetric TUNEL System, Promega). Images were obtained using a Zeiss LSM 780 upright confocal/two-photon combined microscope and analysed using Fiji/ImageJ. Cell counting was performed manually using the FIJI plugin Cell Counter.

T-ALL cell number and cell cycle analysis

Bone marrow from human T-ALL xenotransplanted, untreated and treated mice was harvested and stained with DAPI (Invitrogen) and FITC mouse anti-Ki-67 set (BD Biosciences), according to the manufacturer's instructions. Cells were analysed by FACS and absolute numbers were obtained using reference beads as described in36.

Europe PMC Funders Author Manuscripts

Osterix quantification

T-ALL engraftment and infiltration was confirmed via peripheral blood sampling and/or tibia puncture. Once mice presented with signs of ill health (as described earlier), mice were euthanized and bones digested with a DNAse I/Collagenase (Sigma) solution. The total number of Osx/GFP$^+$ cells was assessed by flow cytometry analysis using counting beads (CountBright, Life Technologies).

Human trephine histology

Samples were obtained from patients after informed consent had been obtained, under full ethical approval by the Peter MacCallum Cancer Centre Human Research Ethics Committee. De-waxed human trephine biopsy sections (3μM) were stained with osteocalcin antibody (Abcam ab93876, Cambridge, UK), counterstained and mounted for viewing. All areas of each section were monitored for visible osteoblasts.

Statistics

The sample size required for the experiments was estimated based of the results of preliminary data. Blinding or randomisation for animal experiments were not necessary due to the nature of the experiments. Statistical differences between the means of two data groups was determined by using two-tailed unpaired Student's *t* test, and *p* values <0.05 were considered significant. Multiple group comparisons were performed using ANOVA with a Bonferroni correction, *p* values <0.05 were considered significant.

Europe PMC Funders Author Manuscripts

Extended Data

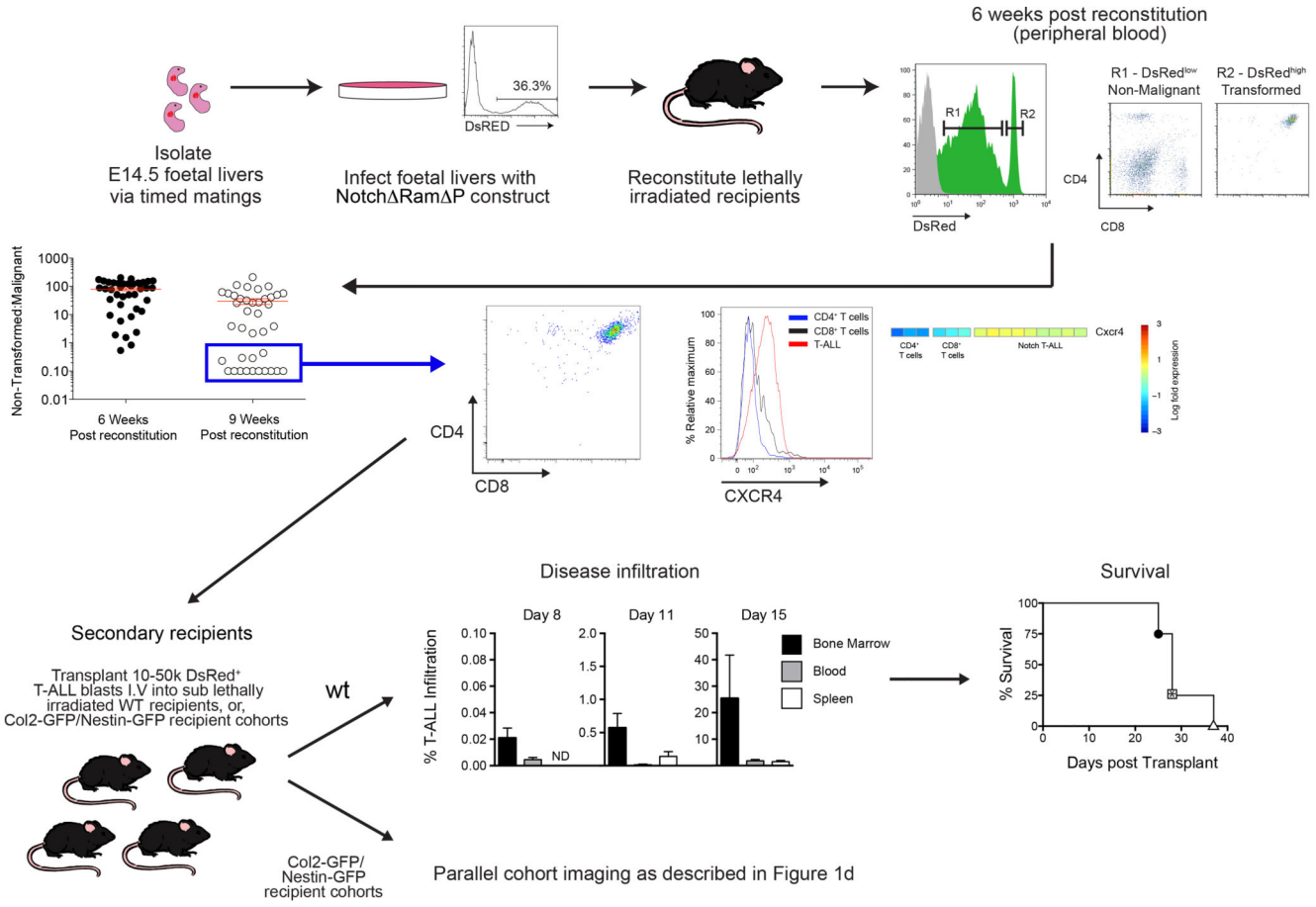

Extended Data Figure 1. T-ALL disease experimental model.

Foetal liver single cell suspensions were isolated from E14.5 wild type embryos and transduced with DsRed alone or DsRed with NotchICNΔRamΔP then transplanted into primary lethally irradiated recipient mice. Recipient mice typically accumulated $CD4^+CD8^+$ cells in the peripheral blood from 4 weeks post transplant. Transformed leukaemic cells could be distinguished from non-malignant cells based on DsRed expression levels, where $DsRED^{lo}$ cells were transduced with the Notch construct yet were non malignant as they had not yet acquired secondary mutations to drive leukaemogenesis, whereas $DsRed^{hi}$ cells were fully malignant. $DsRed^{lo}$ cells contained single positive $CD4^+$ and $CD8^+$ T cell populations, whereas $DsRed^{hi}$ cells had predominantly the leukaemic $CD4^+CD8^+$ phenotype. The accumulation of transformed leukaemic populations displayed large variation over time as shown in the ratio of transformed to non-malignant cells in peripheral blood of primary recipient mice at 6 and 9 weeks. When $DsRed^{hi}$ cells dominated peripheral cell populations, mice were burdened with typical $CD4^+CD8^+$ T-ALL (now simply referred to as $DsRed^+$). When primary recipient mice displayed enlarged lymph nodes and/or spleen, they were euthanized and $DsRed^+$ cells were harvested, stored frozen and transplanted into secondary recipients. CXCR4 expression was measured in $CD4^+$ T cells, $CD8^+$ T cells and T-ALL by flow cytometry (T-ALL from four primary donors) and microarray gene expression analysis

Europe PMC Funders Author Manuscripts

(triplicate biological replicates are shown for control T cells, and samples from nine individual secondary recipients injected with 5 independent primary T-ALL samples). To track disease progression, 10,000 primary T-ALL cells were transplanted into cohorts of sub-lethally irradiated secondary recipient mice. Secondary transplanted cells colonized the bone marrow primarily, before spreading to peripheral organs and blood (n = 4 mice per time point) and developed disease more rapidly and synchronously than primary recipients as injected cells were already transformed. Secondary recipients survived for up to 38 days (shown are survival data of mice injected with 4 independent primary T-ALL samples [●, ❑, * and Δ], n = 2 mice per primary sample). In selected cases, secondary T-ALL blasts were transplanted into tertiary recipients, which developed disease more rapidly but showed similar responses to chemotherapy. The primary samples used in this study were from primary recipients 151, 907, B2M2, B2M3, B2M10, B3M3 and B3M30. This nomenclature refers to the mouse numbering from three independent foetal liver transductions. 1st transduction: mouse 151 and 907, 2nd transduction (B2): mouse 2, 3 and 10; 3rd transduction (B3): mouse 3 and mouse 30.

Europe PMC Funders Author Manuscripts

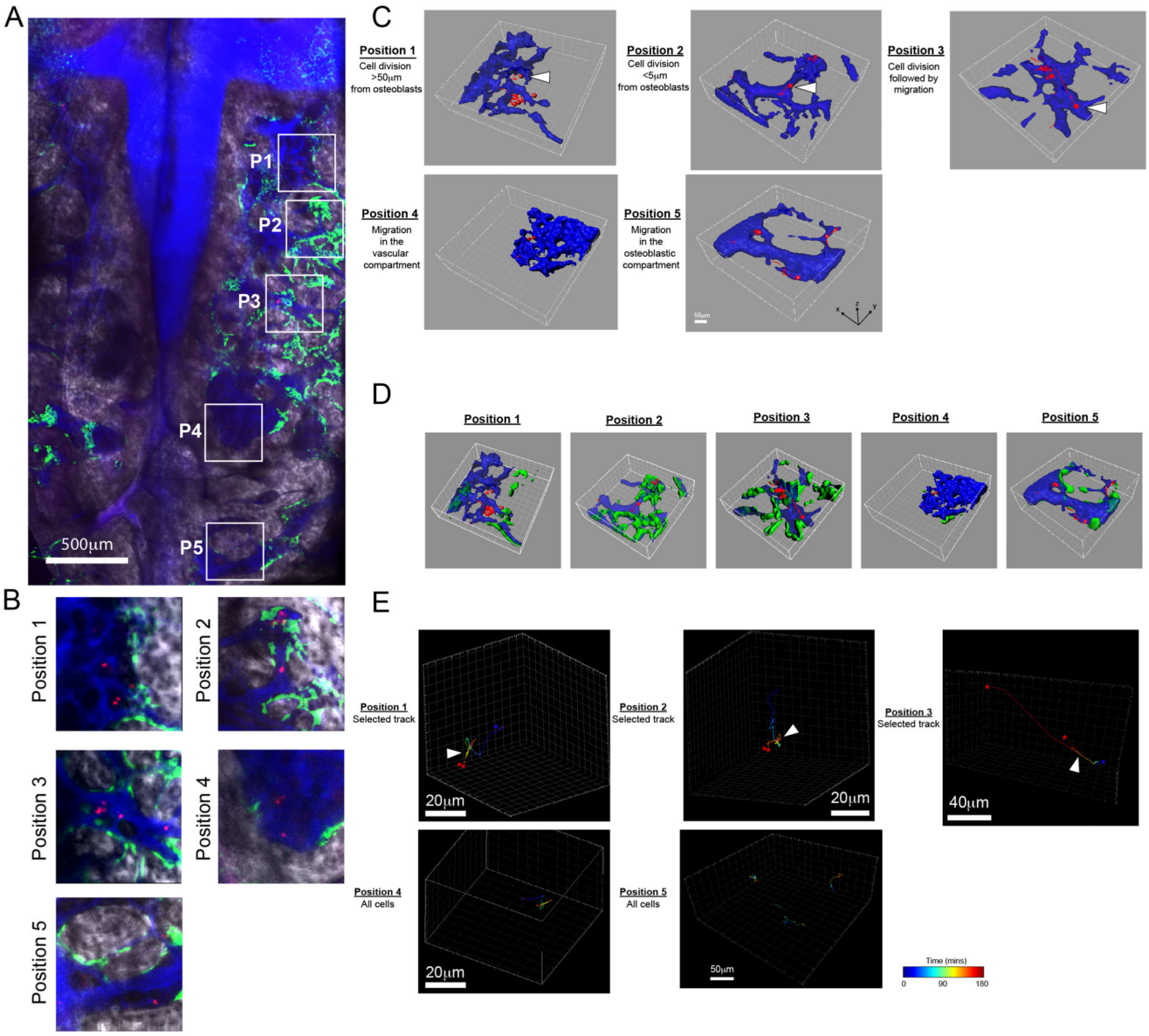

Extended Data Figure 2. Four-dimensional multi-position imaging of leukaemia cells in the BM space.

(A) Representative maximum projection tilescan of a Col2.3-GFP recipient mouse (from figure 2) 12 days post-transplant of DsRed^{+} T-ALL. Red: T-ALL cells; green: GFP^{+} osteoblastic cells; blue: blood vessels; grey: bone collagen. (**B**) Individual positions (framed in A) were selected and imaged at three-minute intervals for three hours to measure cell migration and division. Shown here are a single time frame/position. For full time-lapse data see Supplementary Video 2 (**C**) 3D rendering of the three dimensional tracks of individual leukaemia cells, measured using semi-automated tracking (red), overlaid to vasculature (blue). Spheres represent the beginning of each track. (**D**) Data from C is shown with osteoblasts included in green. (**E**) Tracks from C colour-coded based on time. Long stretches of the same colour correspond to faster movement, while rapid colour shifts represent slower

movement. Data are representative of >30 time-lapse videos collected from eight secondary recipients injected with three independent primary T-ALL samples.

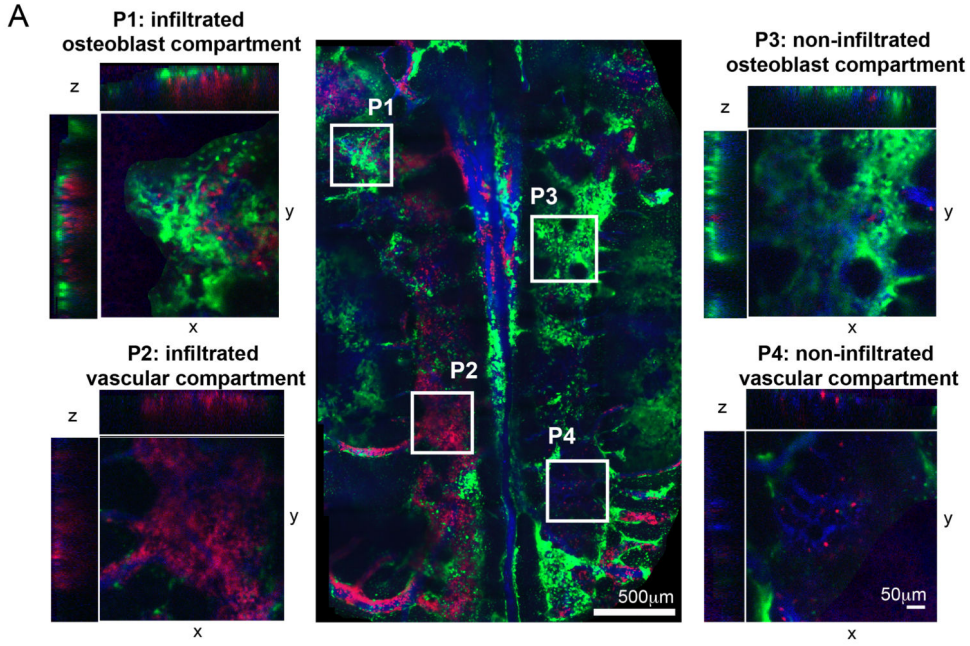

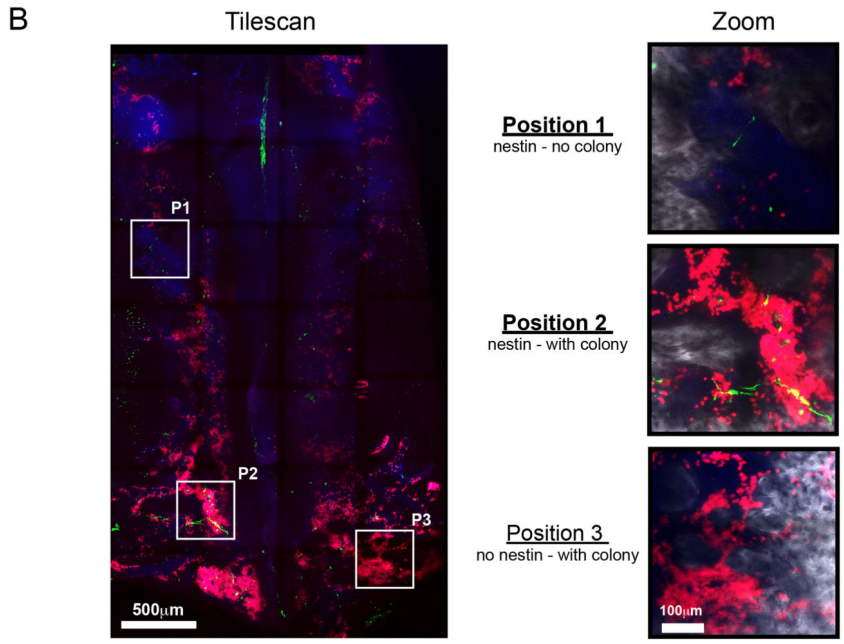

Extended Data Figure 3. T-ALL expansion is not associated with Col2.3-GFP$^+$ osteoblastic cells and Nestin-GFP$^+$ cells.

(A) Representative tilescan of a Col2.3-GFP mouse 15 days post transplantation of T-ALL. Zooms P1-P4 illustrate that the expansion of disease is not associated with the presence or absence of GFP$^+$ osteoblaststic cells. Red: T-ALL, Green: osteoblastic cells, Blue: blood vessels. Image is representative of 5 mice injected with 2 individual T-ALL primary

Europe PMC Funders Author Manuscripts

samples. **(B)** Representative tilescan of a Nestin-GFP mouse 15 days post transplantation of T-ALL. Zooms P1-P3 illustrate that the expansion of disease is not associated with the presence or absence of nestin-GFP$^+$ cells. Red: T-ALL, Green: nestin$^+$ cells, Blue: blood vessels, Grey: bone collagen SHG signal. Image is representative of 3 individual mice.

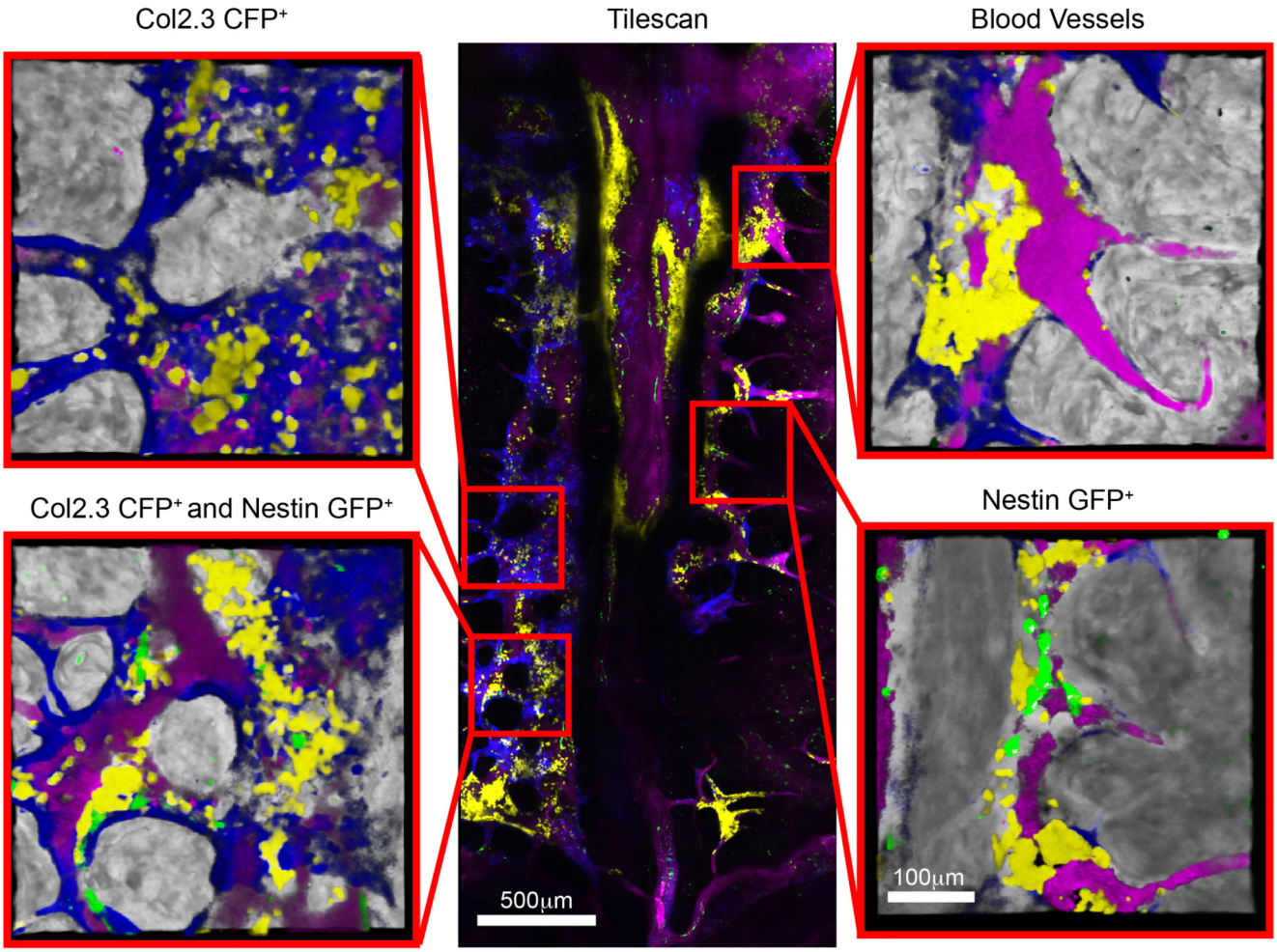

Extended Data Figure 4. T-ALL expansion is not associated with bone marrow areas containing nestin-GFP$^+$, Col2.3-GFP$^+$ cells or any combination of them.

Representative tilescan of a Col2.3-CFP/Nestin-GFP double transgenic mouse 15 days post transplantation of T-ALL. Zooms P1-P3 illustrate that the expansion of disease is not associated with the presence or absence of any combination of Col2.3-CFP$^+$ or Nestin-GFP$^+$ cells. Yellow: T-ALL, Green: Nestin-GFP$^+$ cells, Blue: Col2.3-CFP$^+$ cells, Magenta: Cy5 labelled blood vessels, Grey: bone collagen SHG signal. Image is representative of 4 mice.

Europe PMC Funders Author Manuscripts

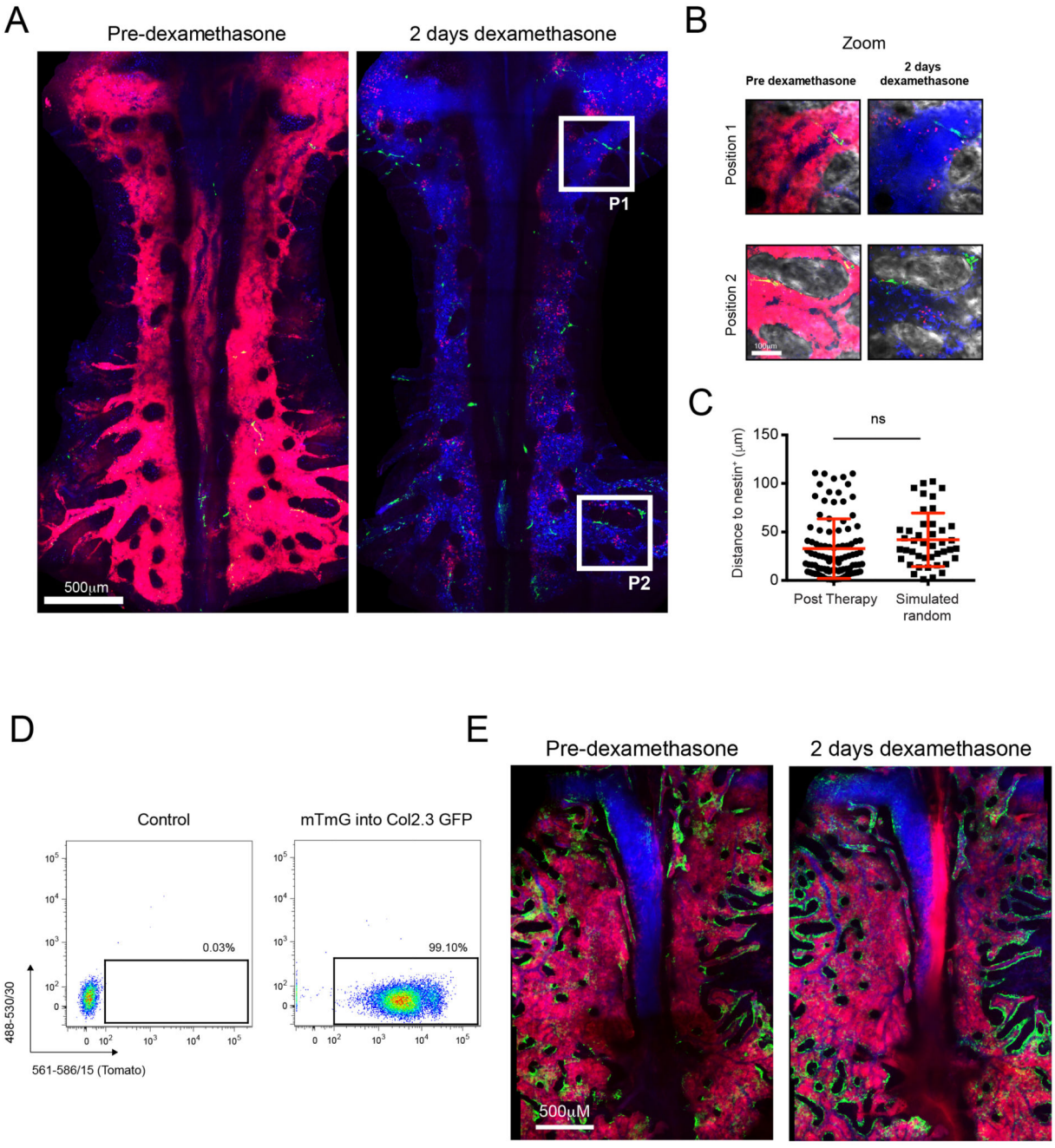

Extended Data Figure 5. Dexamethasone-resistant T-ALL cells do not associate with Nestin-GFP$^+$ cells.

(**A**) Representative nestin-GFP mouse transplanted with T-ALL cells and imaged 18 days post-transplant to confirm complete BM infiltration (left). Tilescan imaging was repeated after two days of treatment with 15mg/kg dexamethasone I.V. (right). (**B**) Magnified view of representative positions, framed in A. (**C**) We observed no preferential positioning of T-ALL surviving cells relative to Nestin$^+$ cells compared to simulated data. Red: T-ALL, Green: Nestin-GFP$^+$ cells, Blue: blood vessels. Data is representative of 4 individual mice injected

with 2 T-ALL primary samples. **(D)** Chimeric mice were generated by transplanting mTmG - tomato^{+} BM into Col2.3-GFP recipients. The high reconstitution efficiency of mTmG cells provided a more robust traceable marker of steady state haematopoiesis for intravital imaging than MigR1-DsRed transduced foetal liver cells (<40% reconstitution, not shown). (**E**) Representative tilescans of mTmG/Col2.3-GFP chimeric mouse performed before, and after three doses of dexamethasone treatment showing that healthy bone marrow is not affected by dexamethasone treatment or sub-lethal irradiation. Red: tomato positive, healthy mTmG BM; green: GFP^{+} osteoblastic cells; blue: blood vessels. n = 2 mice.

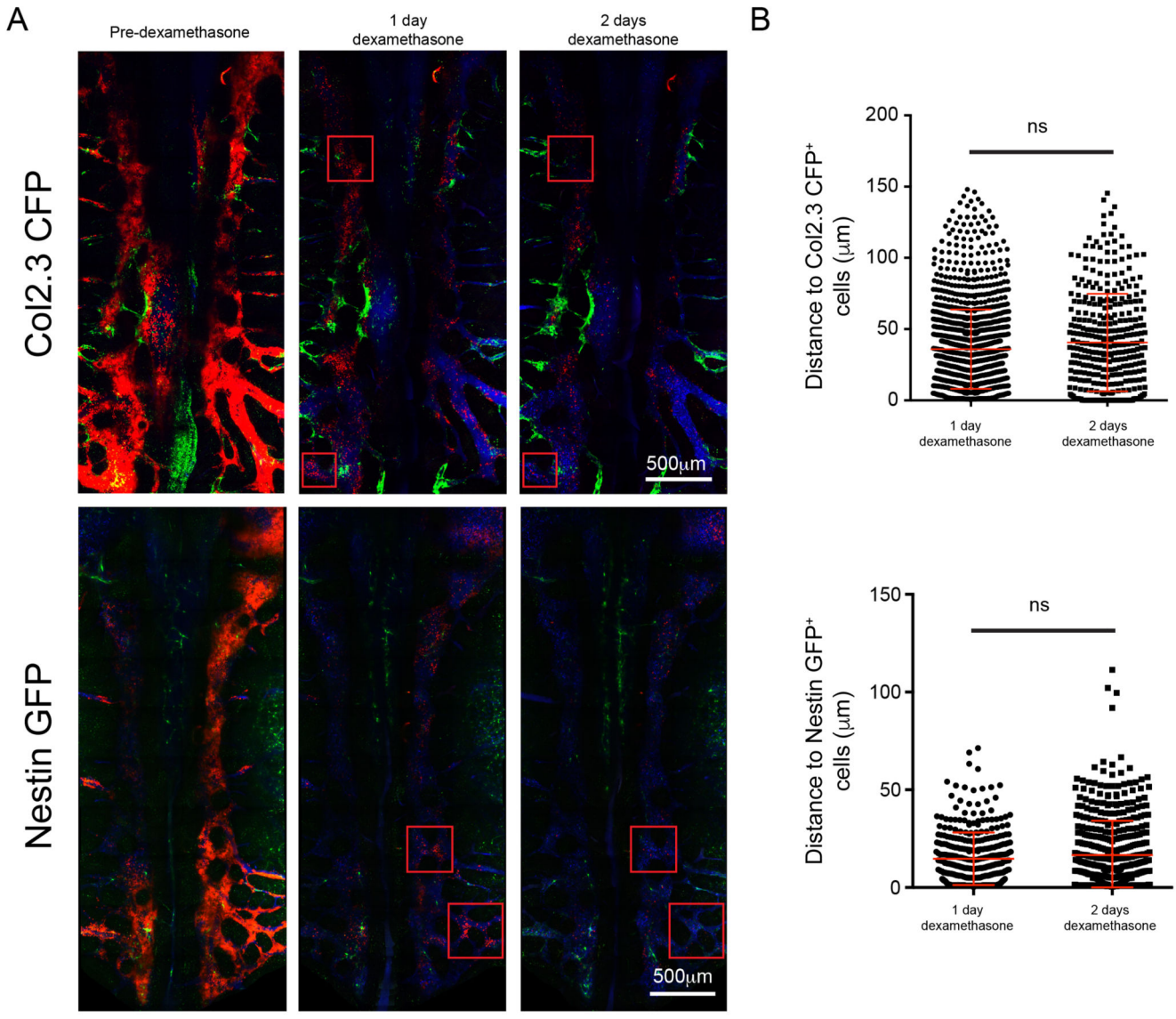

Extended Data Figure 6. Multi-day time course of response to chemotherapy.

(A) Representative maximum projections of tilescans of calvarium bone marrow of one Col2.3-CFP and one Nestin-GFP mouse at 18 days post T-ALL transplant (pre-treatment) and 1 and 2 days of dexamethasone treatment (15mg/kg). Red squares indicate some areas

Europe PMC Funders Author Manuscripts

of cell loss from day 1 to day 2. **(B)** 3D measurement of the position of surviving cells in mice imaged at both 1 and 2 days of dexamethasone treatment. n = 1499 and 352 T-ALL cells measured to osteoblastic-CFP$^+$ cells at day 1 and day 2, respectively, and 363 and 496 T-ALL cells measured to nestin-GFP$^+$ cells at day 1 and day 2, respectively. Data are representative from 3 individual mice of each genotype. Error bars in B: mean ± S.D.

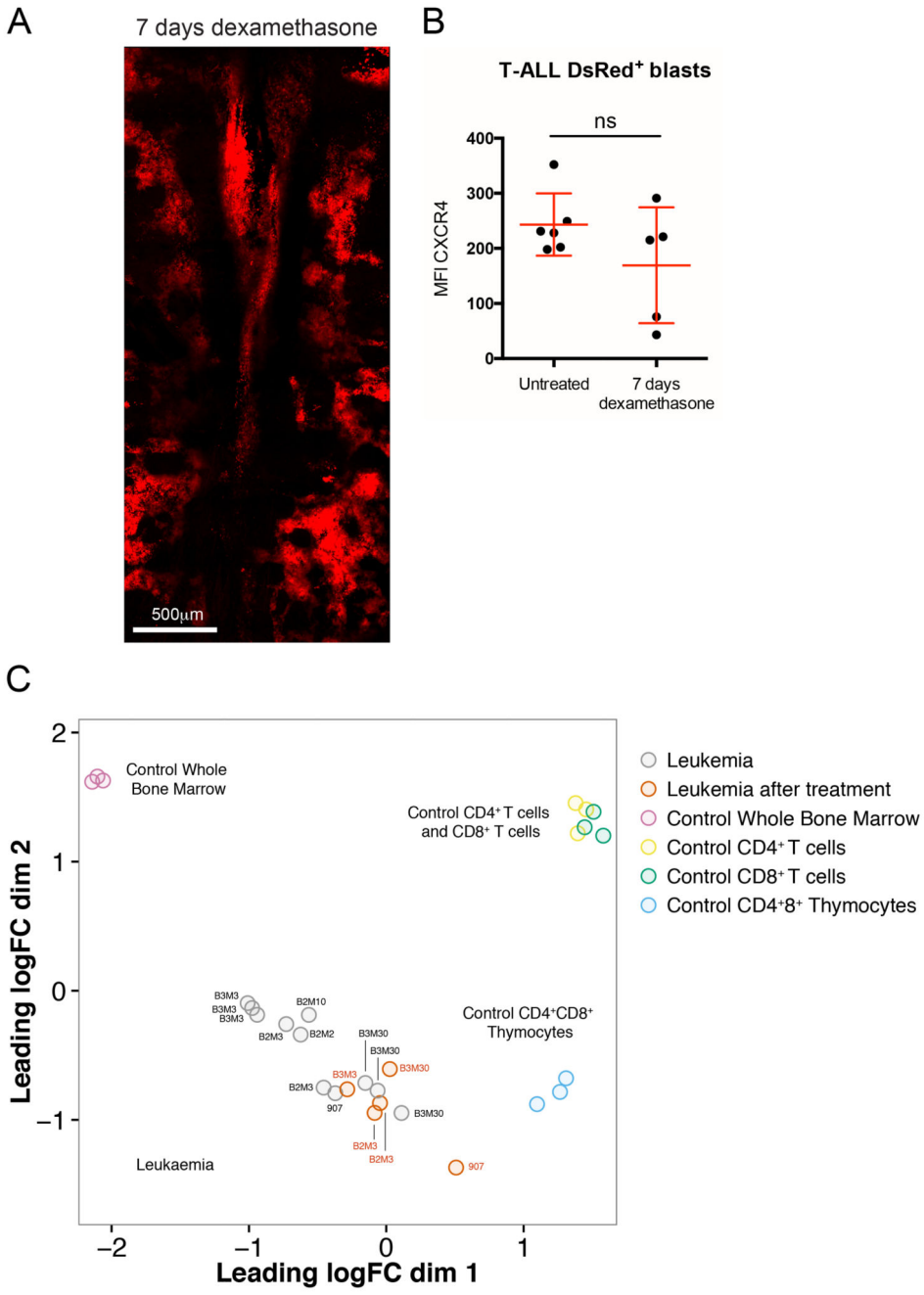

Extended Data Figure 7. Development of resistance to dexamethasone and gene expression-based clustering of leukaemia samples harvested before and after dexamethasone treatment.

(A) Representative maximum projection of tilescan of calvarium bone marrow of a mouse after 7 days of daily dexamethasone treatment (15 mg/kg, I.V.). Red = DsRed^{+} T-ALL cells. Data are representative of 4 independent mice injected with 4 independent T-ALL primary samples. **(B)** Mice with T-ALL were either kept untreated or treated with dexamethasone for 7 days, at which point they were culled and the expression of CXCR4 on T-ALL cells analysed by flow cytometry. There was no statistically significant difference in the mean fluorescence intensity (MFI) of CXCR4 between the two groups. Data are representative of 6 untreated and 5 treated mice, injected with 3 independent T-ALL primary samples. **(C)** Multi-dimensional scaling (MDS) plot of control CD4^{+} T cells, CD8^{+} T cells, CD4^{+}8^{+} thymocytes, whole bone marrow and T-ALL samples with no treatment (grey) or after treatment with dexamethasone (red) based on microarray transcriptomics data for the 1000 most variable genes. The name of the primary T-ALL sample used to inject each mouse is indicated next to the dot marking its position relative to all other samples. This nomenclature refers to the mouse numbering from three independent foetal liver transductions. 1st transduction: mouse 907; 2nd transduction (B2): mouse 2 – B2M2, mouse 3 – B2M3 - and 10 – B2M10; 3rd transduction (B3): mouse 3 – B3M3 - and mouse 30 – B3M30. Control samples are purified by flow cytometry from 3 biological replicate mice and each circle represents an individual sample.

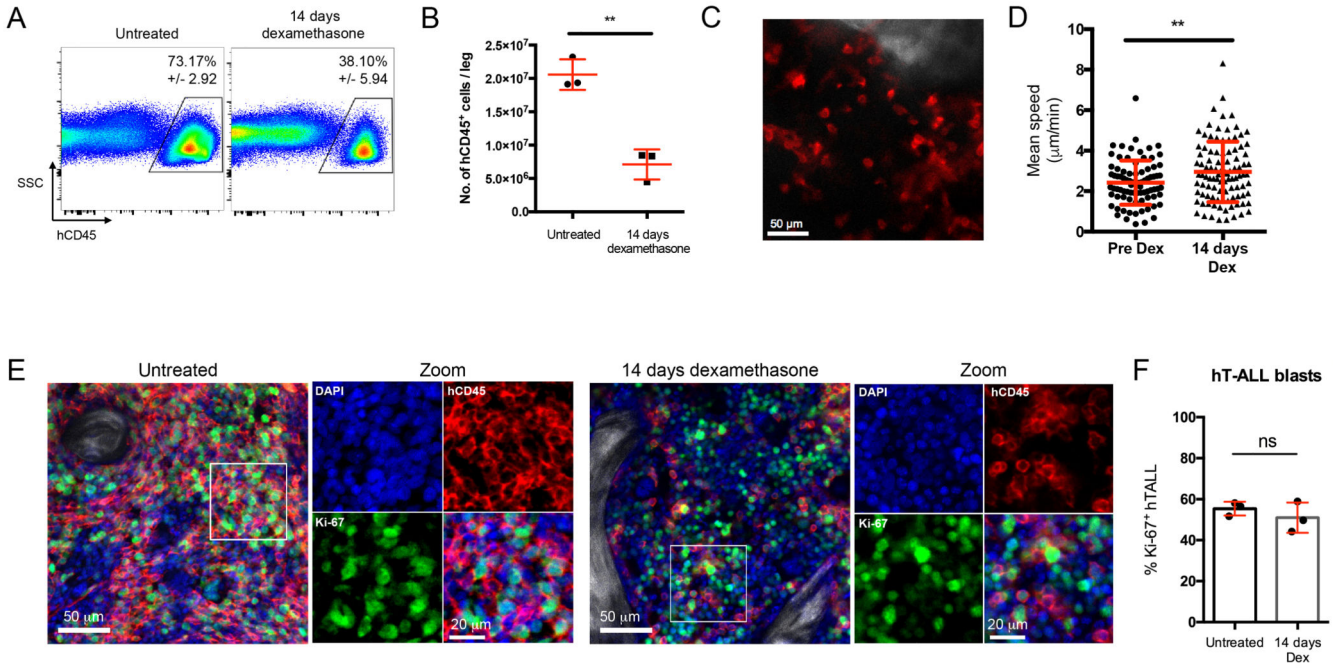

Extended Data Figure 8. Analysis of human T-ALL cells during response to chemotherapy in NSG xenotransplant recipients.

Human T-ALL samples were transplanted into NOD/SCID/γ (NSG) mice and 12 days post transplant, daily dexamethasone treatment at 15mg/kg was initiated. 14 days later, the response was measured by flow cytometry **(A, B)**. For intravital imaging, human T-ALL cells were labelled by injection of 10µg anti-human CD45-PE 15-30 minutes before imaging **(C)**. Cells were imaged at 3 minute intervals for > 60 minutes and migration measured by

manual tracking either before or after dexamethasone treatment **(D)**. Pre dex: $n = 82$ cells from 2 independent mice, 14 days dex: $n = 100$ from 3 independent mice. Error bars = mean +/- S.D. Shown are cells from patient JH, wild type Notch. **(E)** Bone marrow sections were prepared from untreated and treated NSG mice and stained for human CD45 (red) and Ki-67 (green). In addition, nuclei were visualized using DAPI (blue) and bone by second harmonic generation signal (grey). Zooms are of the areas framed by the white boxes on their left. **(F)** Analysis of 2338 (untreated) and 1576 (14 days dex) human $CD45^+$ cells in sections from 3 mice per condition reveals no change in the fraction of proliferating $Ki\text{-}67^+$ cells following dexamethasone treatment.

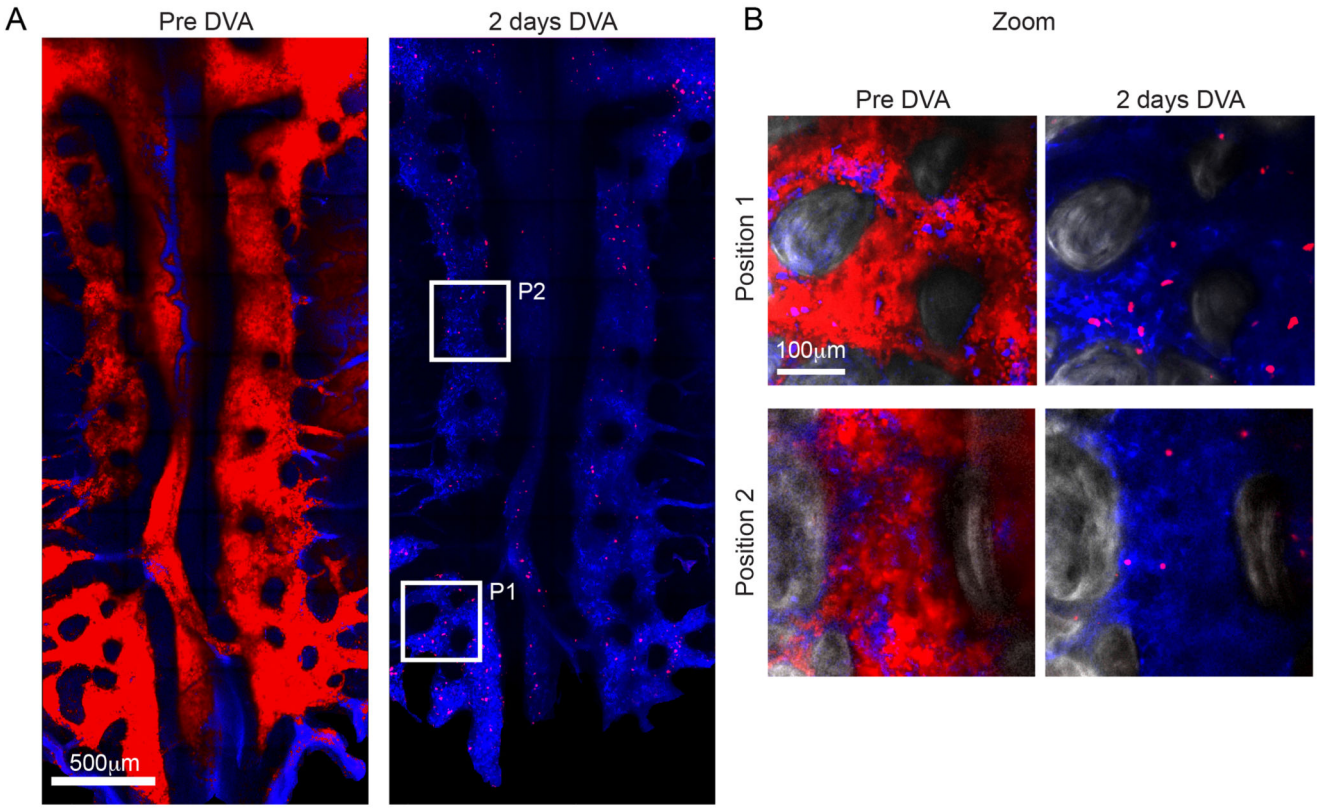

Extended Data Figure 9. Combined dexamethasone, vincristine and L-asparaginase treatment effectively reduces T-ALL burden.

(A) Representative tilescan of a mouse calvarium fully infiltrated with T-ALL (pre DVA) and after 2 days of combination therapy (dexamethasone, vincristine and L-asparaginase – DVA). **(B)** Zooms P1 and P2 illustrate effectiveness of DVA treatment and the small number of surviving T-ALL cells. Red: T-ALL, Blue: blood vessels, Grey: SHG bone collagen. Image is representative of four mice injected with one individual T-ALL secondary sample.

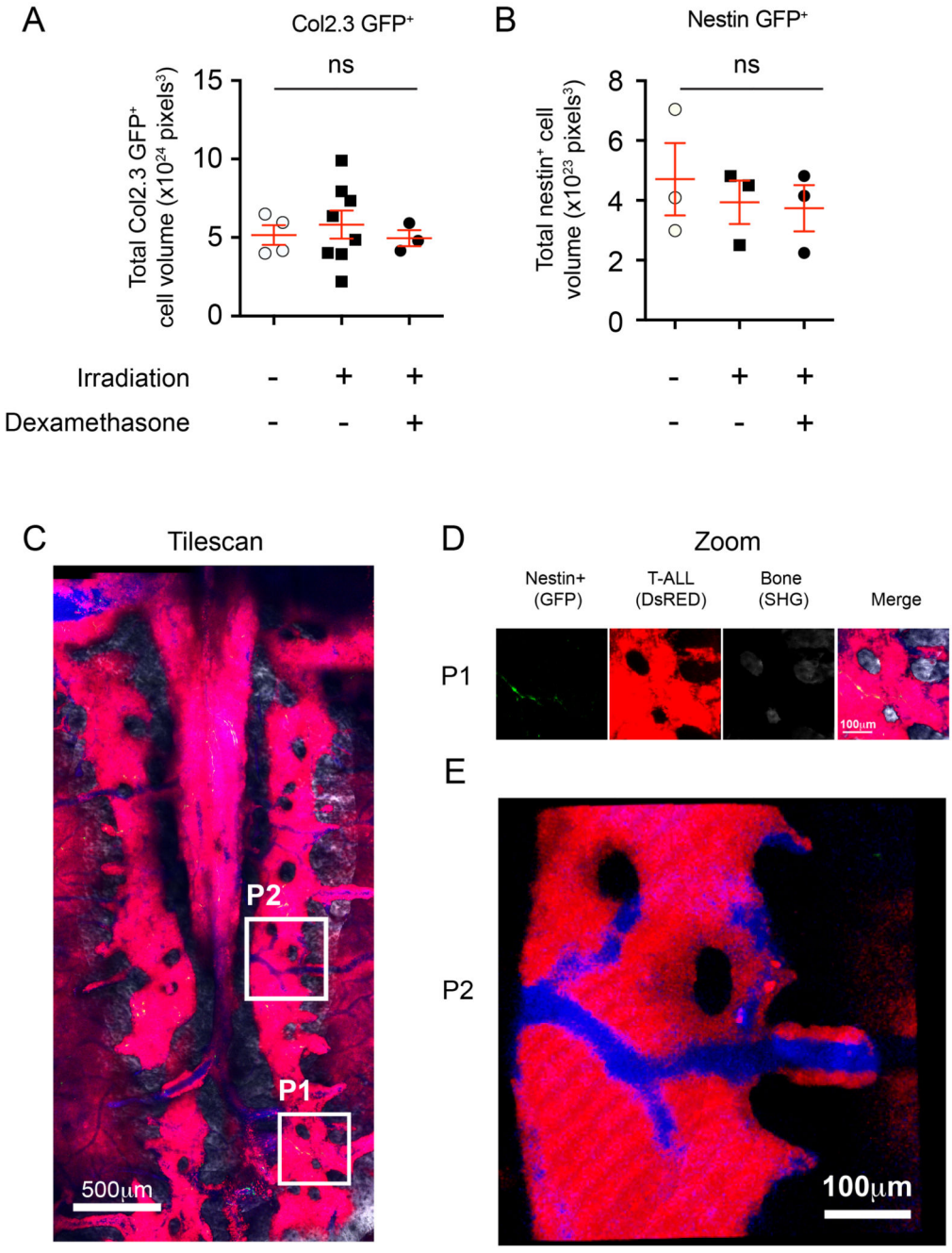

Extended Data Figure 10. Analysis of the response of bone marrow structures to irradiation and dexamethasone treatment and of Nestin-GFP$^+$ cells to T-ALL.

(A) Col2.3-GFP or (**B**) Nestin-GFP mice were treated with combinations of sublethal irradiation (administered >18 days before measurement) or dexamethasone treatment (administered for 2 days before measurement) as indicated. Then, using 3D image analysis of tilescans, the total volume of GFP$^+$ cells was quantified. Groups were analysed using ANOVA with Bonferroni correction for multiple groups. Error bars = Mean +/- S.D. **(C)** Representative tilescan of nestin-GFP mouse transplanted with T-ALL 21 days earlier. At

Europe PMC Funders Author Manuscripts

infiltration levels that eradicated osteoblasts, we still observed healthy nestin-GFP$^+$ cells. **(D)** Higher magnification of area P1 framed in A, with the signal from each channel split for clarity. **(E)** Three dimensional render at higher magnification of area P2 framed in A, showing healthy blood flow within the highly infiltrated BM space. Red: T-ALL, Green: Nestin-GFP$^+$ cells, Blue: blood vessels. Grey: bone collagen SHG signal. $n = 5$ independent mice injected with 2 independent T-ALL primary samples.

Supplementary Material

Refer to Web version on PubMed Central for supplementary material.

Acknowledgements

EH was supported by a fellowship from the European Haematology Association (EHA), and project grant from Bloodwise (12033). DD was supported by the GABBA PhD program (FCT fellowship SFRH/BD/52195/2013). LP was supported by an NHMRC Senior Research Fellowship. HQ is supported by Victorian Cancer Agency Early Career Seed Grant. DB, DP and KF were funded by Cancer Research UK and the Francis Crick Institute. CLC was funded by Bloodwise (12033), HFSP (RGP0051/2011), CRUK (C36195/A1183), BBSRC (BB/I004033/1) KKLF (KKL460) and ERC (337066). We are grateful to Dr. Martin Spitaler and Dr. Debbi Keller (Imperial College FILM facility) for support with microscopy. We also thank Savvas Piperelis, Edgar Ibarguen, Wendy Steel and Helen Goyal (Imperial College CBS facility) for logistical help; Andrew Ivan for support from the Genomics facility; Jane Srivastava and Catherine Simpson for support from the flow cytometry facility; Meaghan Wall (St. Vincent's Hospital) for her advice on the human cytogenetics; Delissa Ibanez (Bitplane) for access to software; Dr. H. Fleming (MIT), Prof. V. Greco (Yale University), Prof. RE Sinden (IC), Dr S. Mostowy (IC) and Dr. P. O'Donovan (Wellcome Trust) for critical feedback on the manuscript.

References

1. Bowers M, et al. Osteoblast ablation reduces normal long-term hematopoietic stem cell self-renewal but accelerates leukemia development. Blood. 2015; 125:2678–2688. DOI: 10.1182/blood-2014-06-582924 [PubMed: 25742698]
2. Colmone A, et al. Leukemic cells create bone marrow niches that disrupt the behavior of normal hematopoietic progenitor cells. Science. 2008; 322:1861–1865. DOI: 10.1126/science.1164390 [PubMed: 19095944]
3. Duan CW, et al. Leukemia propagating cells rebuild an evolving niche in response to therapy. Cancer cell. 2014; 25:778–793. DOI: 10.1016/j.ccr.2014.04.015 [PubMed: 24937459]
4. Hanoun M, et al. Acute myelogenous leukemia-induced sympathetic neuropathy promotes malignancy in an altered hematopoietic stem cell niche. Cell stem cell. 2014; 15:365–375. DOI: 10.1016/j.stem.2014.06.020 [PubMed: 25017722]
5. Ishikawa F, et al. Chemotherapy-resistant human AML stem cells home to and engraft within the bone-marrow endosteal region. Nature biotechnology. 2007; 25:1315–1321. DOI: 10.1038/nbt1350
6. Saito Y, et al. Induction of cell cycle entry eliminates human leukemia stem cells in a mouse model of AML. Nature biotechnology. 2010; 28:275–280. DOI: 10.1038/nbt.1607
7. Schepers K, et al. Myeloproliferative neoplasia remodels the endosteal bone marrow niche into a self-reinforcing leukemic niche. Cell stem cell. 2013; 13:285–299. DOI: 10.1016/j.stem.2013.06.009 [PubMed: 23850243]
8. Zhang B, et al. Altered microenvironmental regulation of leukemic and normal stem cells in chronic myelogenous leukemia. Cancer cell. 2012; 21:577–592. DOI: 10.1016/j.ccr.2012.02.018 [PubMed: 22516264]
9. Jin L, et al. CXCR4 up-regulation by imatinib induces chronic myelogenous leukemia (CML) cell migration to bone marrow stroma and promotes survival of quiescent CML cells. Molecular cancer therapeutics. 2008; 7:48–58. DOI: 10.1158/1535-7163.MCT-07-0042 [PubMed: 18202009]

10. Weisberg E, et al. Inhibition of CXCR4 in CML cells disrupts their interaction with the bone marrow microenvironment and sensitizes them to nilotinib. Leukemia. 2012; 26:985–990. DOI: 10.1038/leu.2011.360 [PubMed: 22182920]
11. Sanda T, et al. Interconnecting molecular pathways in the pathogenesis and drug sensitivity of T-cell acute lymphoblastic leukemia. Blood. 2010; 115:1735–1745. DOI: 10.1182/blood-2009-07-235143 [PubMed: 20007543]
12. Weng AP, et al. Activating mutations of NOTCH1 in human T cell acute lymphoblastic leukemia. Science. 2004; 306:269–271. DOI: 10.1126/science.1102160 [PubMed: 15472075]
13. Pui CH, Robison LL, Look AT. Acute lymphoblastic leukaemia. Lancet. 2008; 371:1030–1043. DOI: 10.1016/S0140-6736(08)60457-2 [PubMed: 18358930]
14. Lo Celso C, et al. Live-animal tracking of individual haematopoietic stem/progenitor cells in their niche. Nature. 2009; 457:92–96. DOI: 10.1038/nature07434 [PubMed: 19052546]
15. Rashidi NM, et al. In vivo time-lapse imaging shows diverse niche engagement by quiescent and naturally activated hematopoietic stem cells. Blood. 2014; 124:79–83. DOI: 10.1182/blood-2013-10-534859 [PubMed: 24850759]
16. Scott MK, Akinduro O, Lo Celso C. In vivo 4-dimensional tracking of hematopoietic stem and progenitor cells in adult mouse calvarial bone marrow. Journal of visualized experiments : JoVE. 2014; :e51683.doi: 10.3791/51683 [PubMed: 25225854]
17. Kalajzic I, et al. Use of type I collagen green fluorescent protein transgenes to identify subpopulations of cells at different stages of the osteoblast lineage. Journal of bone and mineral research : the official journal of the American Society for Bone and Mineral Research. 2002; 17:15–25. DOI: 10.1359/jbmr.2002.17.1.15
18. Paic F, et al. Identification of differentially expressed genes between osteoblasts and osteocytes. Bone. 2009; 45:682–692. DOI: 10.1016/j.bone.2009.06.010 [PubMed: 19539797]
19. Mendez-Ferrer S, et al. Mesenchymal and haematopoietic stem cells form a unique bone marrow niche. Nature. 2010; 466:829–834. DOI: 10.1038/nature09262 [PubMed: 20703299]
20. Inaba H, Pui CH. Glucocorticoid use in acute lymphoblastic leukaemia. The Lancet Oncology. 2010; 11:1096–1106. DOI: 10.1016/S1470-2045(10)70114-5 [PubMed: 20947430]
21. Mullighan CG, et al. Genomic analysis of the clonal origins of relapsed acute lymphoblastic leukemia. Science. 2008; 322:1377–1380. DOI: 10.1126/science.1164266 [PubMed: 19039135]
22. Lassailly F, Foster K, Lopez-Onieva L, Currie E, Bonnet D. Multimodal imaging reveals structural and functional heterogeneity in different bone marrow compartments: functional implications on hematopoietic stem cells. Blood. 2013; 122:1730–1740. DOI: 10.1182/blood-2012-11-467498 [PubMed: 23814020]
23. Visnjic D, et al. Hematopoiesis is severely altered in mice with an induced osteoblast deficiency. Blood. 2004; 103:3258–3264. DOI: 10.1182/blood-2003-11-4011 [PubMed: 14726388]
24. Krevvata M, et al. Inhibition of leukemia cell engraftment and disease progression in mice by osteoblasts. Blood. 2014; 124:2834–2846. DOI: 10.1182/blood-2013-07-517219 [PubMed: 25139351]
25. Khorshed RA, et al. Automated identification and localization of hematopoietic stem cells in 3D intravital microscopy data. Stem Cell Reports. 2015
26. Muzumdar MD, Tasic B, Miyamichi K, Li L, Luo L. A global double-fluorescent Cre reporter mouse. Genesis. 2007; 45:593–605. DOI: 10.1002/dvg.20335 [PubMed: 17868096]
27. Rodda SJ, McMahon AP. Distinct roles for Hedgehog and canonical Wnt signaling in specification, differentiation and maintenance of osteoblast progenitors. Development. 2006; 133:3231–3244. DOI: 10.1242/dev.02480 [PubMed: 16854976]
28. Hawkins ED, et al. Lethal giant larvae 1 tumour suppressor activity is not conserved in models of mammalian T and B cell leukaemia. PLoS One. 2014; 9:e87376.doi: 10.1371/journal.pone.0087376 [PubMed: 24475281]
29. Aster JC, et al. Essential roles for ankyrin repeat and transactivation domains in induction of T-cell leukemia by notch1. Molecular and cellular biology. 2000; 20:7505–7515. [PubMed: 11003647]
30. Real PJ, et al. Gamma-secretase inhibitors reverse glucocorticoid resistance in T cell acute lymphoblastic leukemia. Nature medicine. 2009; 15:50–58. DOI: 10.1038/nm.1900

31. Chiu PP, Jiang H, Dick JE. Leukemia-initiating cells in human T-lymphoblastic leukemia exhibit glucocorticoid resistance. Blood. 2010; 116:5268–5279. DOI: 10.1182/blood-2010-06-292300 [PubMed: 20810926]

32. Lo Celso C, Lin CP, Scadden DT. In vivo imaging of transplanted hematopoietic stem and progenitor cells in mouse calvarium bone marrow. Nature protocols. 2011; 6:1–14. DOI: 10.1038/nprot.2010.168 [PubMed: 21212779]

33. Preibisch S, Saalfeld S, Schindelin J, Tomancak P. Software for bead-based registration of selective plane illumination microscopy data. Nature methods. 2010; 7:418–419. DOI: 10.1038/nmeth0610-418 [PubMed: 20508634]

34. Carvalho BS, Irizarry RA. A framework for oligonucleotide microarray preprocessing. Bioinformatics. 2010; 26:2363–2367. DOI: 10.1093/bioinformatics/btq431 [PubMed: 20688976]

35. Ritchie ME, et al. limma powers differential expression analyses for RNA-sequencing and microarray studies. Nucleic acids research. 2015; 43:e47.doi: 10.1093/nar/gkv007 [PubMed: 25605792]

36. Hawkins ED, et al. Measuring lymphocyte proliferation, survival and differentiation using CFSE time-series data. Nature protocols. 2007; 2:2057–2067. DOI: 10.1038/nprot.2007.297 [PubMed: 17853861]

Europe PMC Funders Author Manuscripts

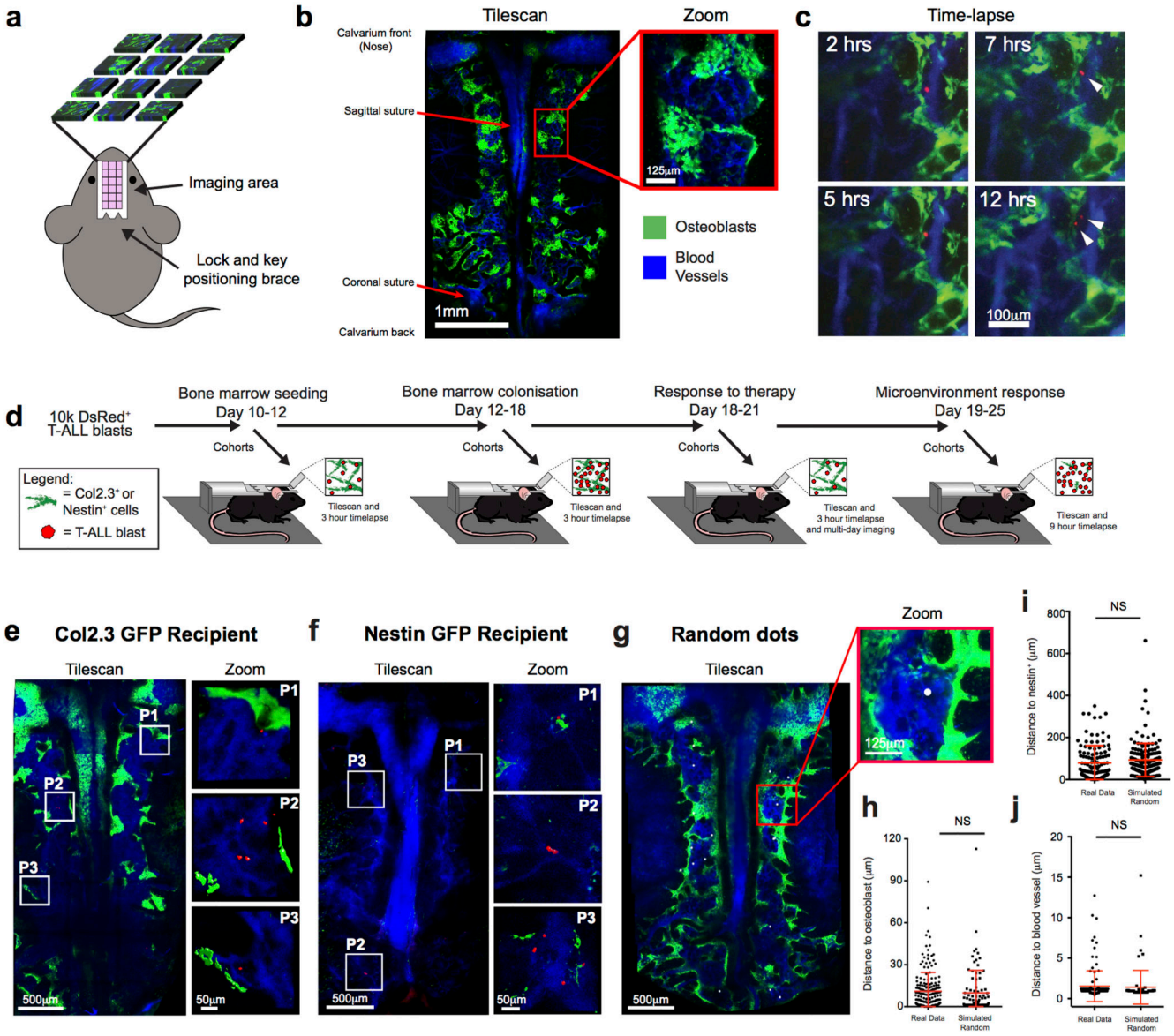

Figure 1. Experimental set up and T-ALL BM seeding

(a) Image data sets were formed of multiple, overlapping z-stacks covering the entire calvarium BM space. (**b**) Tilescans preserve single cell resolution. (**c**) Long-term single cell time-lapse (14 hours). Arrows: division and daughter cells. (**d**) Intravital imaging schedule. (**e** and **f**) Representative maximum projection tilescans showing T-ALL distribution in Col2.3-GFP (**e**) and nestin-GFP (**f**) recipient mice calvarium bone marrow, and corresponding high-magnification 3D renders. (**g**) Simulated cells (white) were randomly distributed within BM space, for control positional measurements. (**h-j**) T-ALL cell location relative to osteoblasts (**h**), nestin cells (**i**) and blood vessels (**j**) compared to randomly positioned dots overlaid on tilescans. Red: T-ALL cells; green: osteoblasts/nestin cells; blue: vasculature. $n = 190$, 117, 135 cells and 91, 168, 70 random dots, respectively in h, i, j; data

Europe PMC Funders Author Manuscripts

representative of/pooled from seven (e, f, h, i) and four independent mice (biological replicates) injected with cells from two independent primary donors. Error bars: mean±S.D.

Europe PMC Funders Author Manuscripts

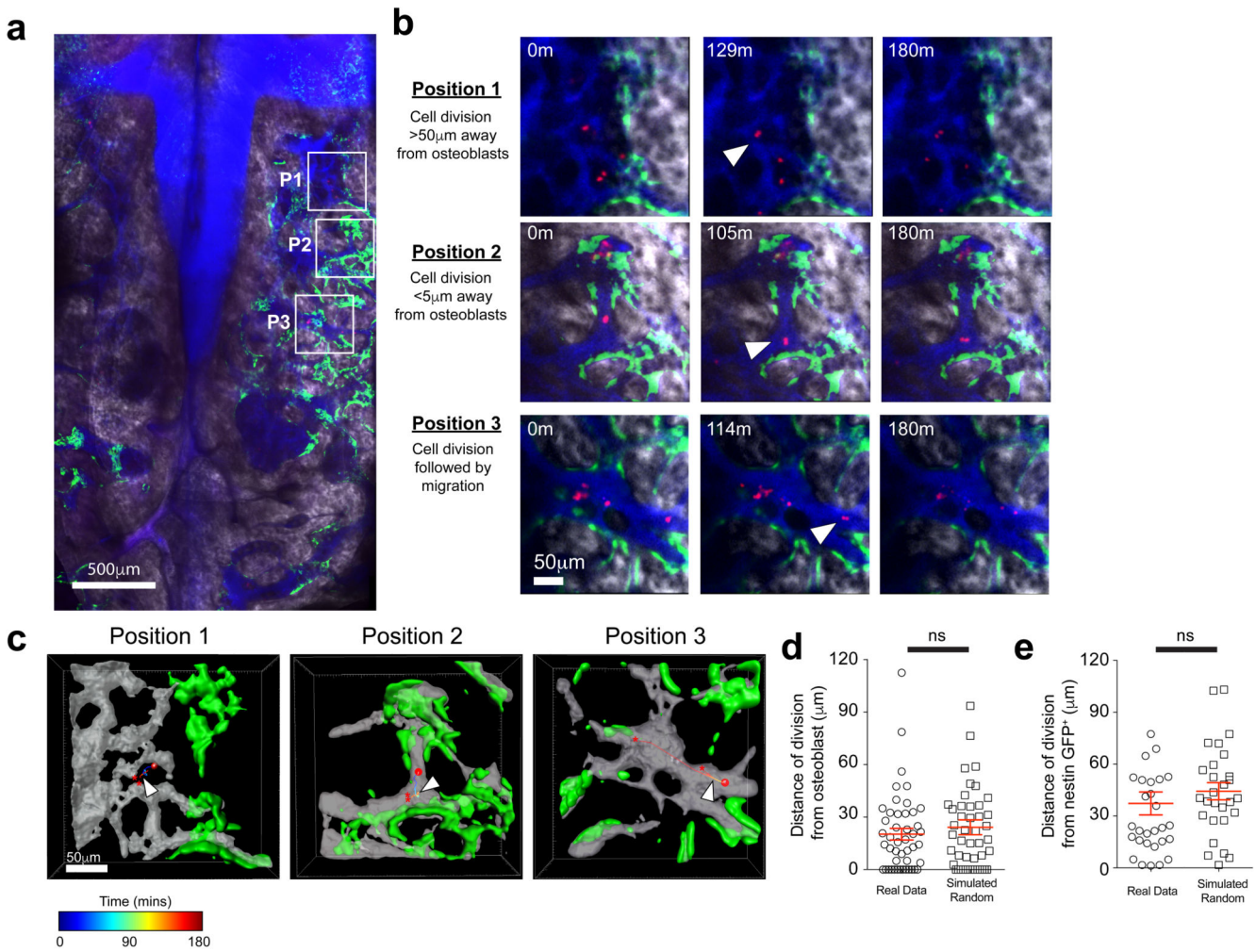

Figure 2. Four-dimensional imaging of leukaemia interactions in BM.

(a) Maximum projection tilescan of a Col2.3-GFP recipient mouse 12 days post-transplant of T-ALL cells. (**b**) Individual positions (framed in a) were imaged at three-minute intervals for three hours. Red: T-ALL cells; green: osteoblasts; blue: vasculature; grey: bone; arrows: mitosis. (**c**) 3D cell tracks (temporally colour-coded) of individual leukaemia cells. Grey: vasculature; green: osteoblasts; red spheres: T-ALL cells at beginning of imaging period; *: finishing position of daughter cells; arrows: mitosis. (**d, e**) Position of mitosis relative to (d) GFP^+ osteoblasts ($n = 46$) or (e) nestin cells ($n = 30$) compared to randomly generated dots ($n = 48$ and 28 respectively). Data in a-d are representative of/pooled from eight mice (biological replicates) injected with T-ALL isolated from three primary donors. Data in e are pooled from four individual mice (biological replicates) injected with T-ALL from two primary donors. Error bars: mean±SEM.

Europe PMC Funders Author Manuscripts

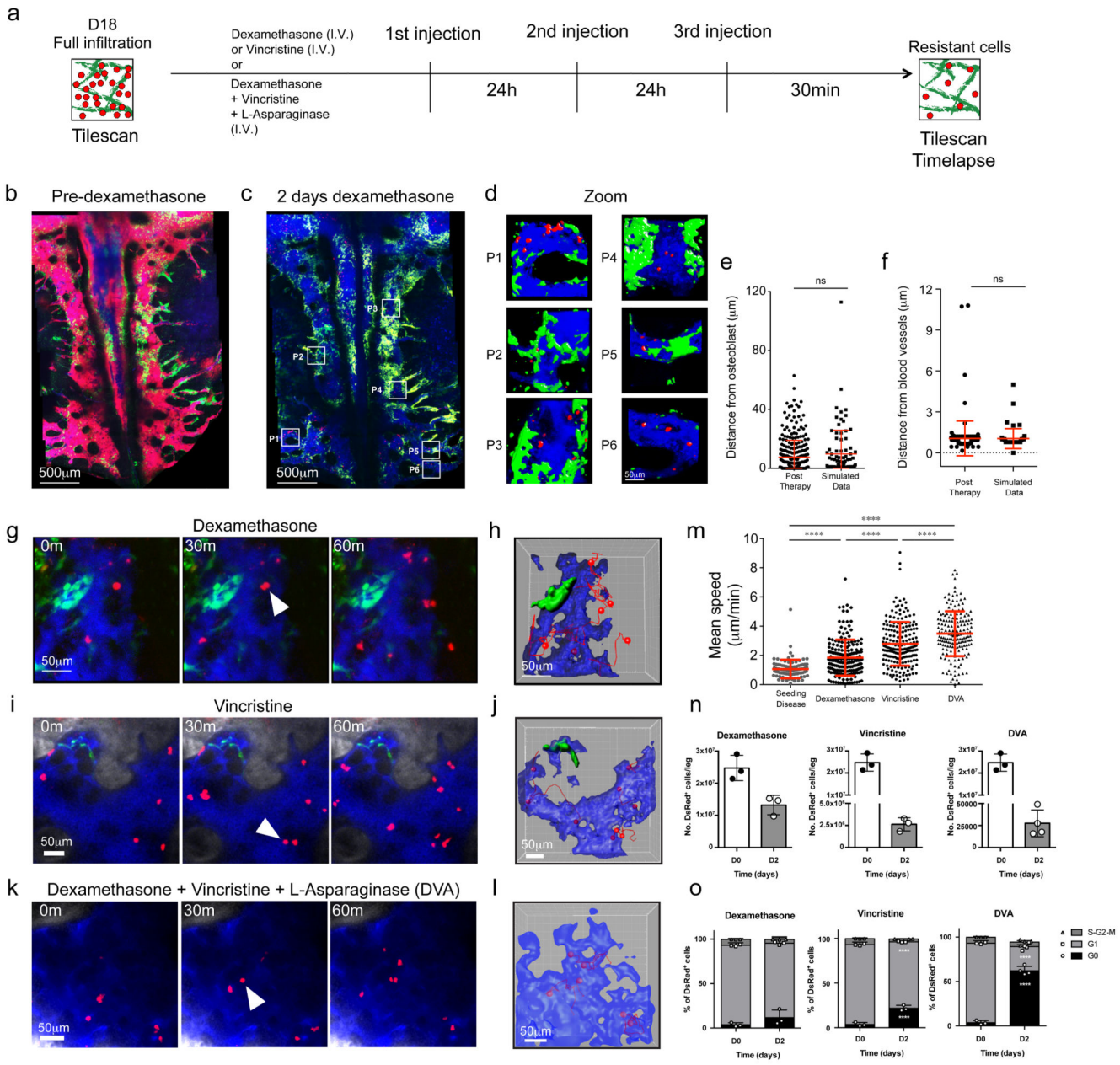

Figure 3. Multi-day imaging of chemotherapy.

(a) Intravital microscopy and treatment schedule. **(b)** Representative maximum projection of Col2.3-GFP calvarium bone marrow 18 days post T-ALL transplant and **(c)** of the same mouse after 2 days of dexamethasone treatment (high-magnification 3D renders of boxed areas shown in **d). (e, f)** Measurement of surviving cells position relative to the closest (**e**) osteoblastic cell (*n*: 303 real and 91 artificial cells) or (**f**) blood vessel (*n*: 143 real and 55 artificial cells). b-f: data representative of/pooled from five mice with T-ALL cells from two primary donors. **(g-l)** Positions imaged at three-minute intervals for three hours in mice treated with dexamethasone (g), vincristine (i) and dexamethasone, vincristine and L-asparaginase (DVA) (k). Arrows: mitosis; green: osteoblastic (g) or nestin cells (i); blue:

Europe PMC Funders Author Manuscripts

vasculature; red: T-ALL cells, grey: bone (i, k). Corresponding cell tracks (red lines) for each treatment are in **h, j, l**. (**m)** Mean speed of cells at early disease and with dexamethasone, vincristine or DVA treatment (n = 91, 184, 199 and 180 cell tracks, respectively). Data pooled from seven early infiltrated, three dexamethasone, five vincristine and four DVA treated mice (biological replicates) from eight independent experiments using T-ALL from two primary donors (early infiltration and dexamethasone treatment), one primary and two secondary donors (vincristine) and one secondary donor (DVA). Cell number **(n)** and cell cycle analysis **(o)** before (D0) and after treatment (D2). Data are pooled from three mice (biological replicates) per time point, injected with T-ALL from one secondary donor. Error bars: mean±S.D.

Europe PMC Funders Author Manuscripts

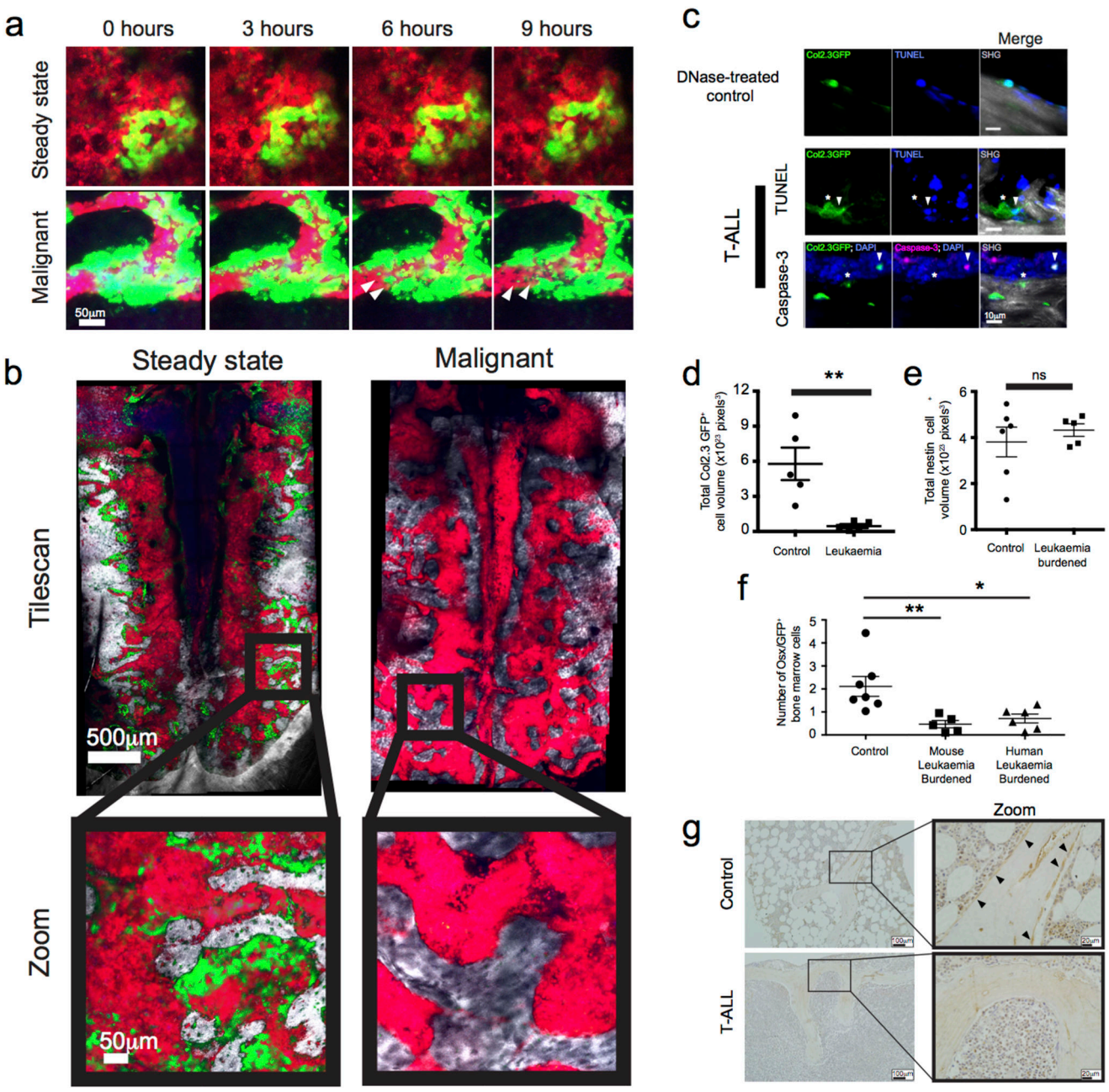

Figure 4. T-ALL rapidly remodels the endosteal niche

(a) 9-hour time-lapse of Col2.3GFP mice calvaria (green: GFP^+ osteoblasts) transplanted with tomato+ bone marrow (red) >8 weeks earlier (upper panels) or $DsRed^+$ T-ALL blasts 19 days earlier (lower panels). Arrows: osteoblastic membrane blebbing. **(b)** Representative tilescans of Col2.3-GFP recipients during steady state haematopoiesis (left) or in malignant state (>22 days T-ALL, right). Bottom panels: high-magnification of boxed areas. Grey: bone; green: osteoblasts; blue: vasculature. Data representative of five healthy and malignant mice. **(c)**Bone sections from Col2.3GFP mice stained for TUNEL or cleaved caspase-3. DNAse pre-treated sections (top) were TUNEL positive control. Grey: bone; green: GFP;

blue: TUNEL/DAPI; purple: cleaved caspase-3; arrows: apoptotic osteoblasts; asterisks: surviving osteoblasts. Representative from three heavily infiltrated mice (biological replicates) injected with T-ALL from two primary donors. **(d)** Quantified osteoblast volume from tilescans shown in (b). **(e)** Quantified nestin volume in Nestin-GFP$^+$ mice 22-25 days post T-ALL transplant. a, b, d e: n = 6/5 mice (biological replicates) from three independent experiments and T-ALL from two primary donors. (**f**) Osterix-GFP$^+$ cells quantified by flow cytometry in mice transplanted with murine and human T-ALL primary cells, at high tumour burden. n = 7 control mice, 5 mice with murine T-ALL from two primary donors and 6 mice with primary human T-ALL from two independent donors. (**g**) BM trephine biopsies from healthy or T-ALL patients immunostained for osteocalcin (brown). Data shown are representative of three healthy controls and four T-ALL patients (biological replicates) with >75% BM blast infiltration. Error Bars = mean±SEM.